Sonoporation and Impedance Spectroscopy for the Assistance with and Observation of Development of Healthier Embryos and Fetuses

A THESIS SUBMITTED TO THE GRADUATE DIVISION OF THE UNIVERSITY OF HAWAIʻI AT MĀNOA IN PARTIAL FULFILLMENT OF THE REQUIREMENTS FOR THE DEGREE OF

MASTER OF SCIENCE

IN

Electrical Engineering

August 2017

by

Kainalu Matthews

Thesis Committee:

Aaron Ohta, Chairperson
Johann Urschitz
Wayne Shiroma

Keywords: Sonoporation, Impedance spectroscopy, *Artemia*, Placenta, Gene delivery, Ultrasound

Acknowledgements

In this section I will betray the third person rule as a colleague of mine did previously.

In reality I have no one to thank since I did this all by myself, just kidding...To say that that this thesis has been difficult would be a massive understatement, and quite frankly this journey began before I was admitted to the Masters program here at the University of Hawai‘i at Mānoa (UHM). There is too many people to thank for the achievements that I have accomplished in my academic life thus far, but I will try my best to thank everyone as best I can.

Mr. Darren Kamalu, the crazy physics teacher in high school who introduced us to the world of conspiracy theories, thank you so much for also teaching us about Nikola Tesla (I guess the math and physics were important too). I will never forget about “jaggies”.

Dr. Joshua Kaakua, Dr. Herb Schroeder, Dr. Bubba Lipe, and Kelli Ching, the staff at the Native Hawaiian Mentorship Program (NHSEMP) and the Alaska Native Science and Engineering Mentorship Program (ANSEP), as well as all my lifelong firends in these programs (too much to list here), thank you all so much for teaching me that there is no shame in asking for help. It was because of your programs I sincerely discovered my passion for engineering.

Arif, Marlee, Haide, Julian, Isaac, Diana, Matt, Anthony, Ryan, Kent, Kareem, Melvin, Andy, Carol, Kelson and other MNM/MMRL/IBR staff, colleagues, and children thank you for the friendship and hours of bad talking my advisors which I will be praising in the following paragraphs. Let us plan a trip and travel together soon.

Dr. Aaron Ohta, my advisor and friend, thank you so much for giving me a chance to do research with you all those years in my undergrad. I guess you liked the torture of mentoring me

so much that you agreed to keep me on as a grad student! I read Andy‘s thesis and saw that you went surfing with him, seems like we need more surf sessions...

Dr. Wayne Shiroma, another advisor and friend, thank you for saying no to me when I first asked to join your research team with Aaron. You taught me dilligence and perservereance with all those intense research meetings, and honestly I would have it no other way. I greatly appreciate your mentorship which taught me not only about engineering, but also how to be a better person.

Dr. Johann Urschitz, just a guy I met recently (kidding), thank you for hiring me and also being an ear throughout my struggles. I appreciate your guidance and jokes, and when I become a billionaire I will buy you 10 new amplifiers.

Mom, Dad, Malorie, Uncles, Aunties, and especially cousin Lopaka, I could not have even come to this point without your support whether it be the 1 AM rides from UH back home, or eating the food you either bought or made for me at home (sorry for eating your food Paka). It was with your support that I made it through these tough years, and I cannot thank you enough.

Lastly, Tutu “Sweets” and my late Papa “Boots” I work hard to make a difference because of the difference you have made, and continue to make in my life.

Grant me the serenity to accept the things I cannot change,

the courage to change the things I can,

and the wisdom to know the difference.

Abstract

Sonoporation and Impedance Spectroscopy for the Assistance with and Observation of Development of Healthier Embryos and Fetuses

by

Kainalu Matthews

Master of Science in Electrical Engineering

University of Hawai‘i, Mānoa
Aaron Ohta, Chair

This thesis presents two separate research projects with an emphasis on developmental biology.

Maternal obesity increases the risk for perinatal complications and predisposes for adult disease. Glucose is one of the main nutrients for a fetus, and it has been shown that the placental Glut1 glucose transporter is upregulated (produced in greater quantities) in obese mothers. By employing sonoporation, we can deliver plasmids directly to placental cells to regulate the Glut1 transporter. This work highlights the steps that were taken to optimize the experimental condition such as the ultrasound parameters used for placental sonoporation in mice.

Viability testing of embryos for bovine and human *in vitro* fertilization remains a challenge. The current procedure is to biopsy the blastocyst cells by first puncturing a hole in the embryo, then cultivating two cells from the blastocyst. The cells give information about the possible aneuploidi’s, or an irregular number of chromosomes within a cell, which may exist within the blastocyst. Impedance spectroscopy is a possible alternative to this highly invasive technique. This work looks at impedance spectroscopy employed for the *Artemia* cysts.

Table of Contents

List of Tables

List of Figures

CHAPTER 1 DEVELOPMENT OF BIOLOGY

Developmental biology is the study of the "development, differentiation, and growth in animals and plants at the molecular, cellular, genetic and evolutionary levels" [1]. Embryogenesis is a small part of developmental biology; however, it is the beginning stage of life for animals therefore is perhaps one of the most important areas of research. For animal development embryogenesis is the study of a fertilized egg cell.

Advances in technology have greatly benefitted the medical field over the course of history. In-vitro fertilization (IVF) [2], magnetic resonance imaging (MRI) [3], and cardiac defibrillators [4] are just several examples of this. IVF is a powerful tool for embryogenesis because it enables for a greater genetic selection prior to development of an embryo. For example, IVF is currently used in the bovine industry to produce cattle which are either optimal for producing milk (e.g. in the dairy industry) or highest quality grade beef (e.g. in the meat industry).

Ultrasound has been used since the 1940's and commonly serves as a diagnostic imaging tool [5]. Recently, the application of ultrasound has been expanded into a different area - as a therapeutic tool. For example, to enable gene transfection of cells within a host or to ablate tissues. Using ultrasound to deliver DNA molecules into cells is known as sonoporation.

The technique of using ultrasound to enable gene transfection is known as sonoporation. In brief, lipid microbubbles coated with DNA are delivered through the bloodstream of a host. Ultrasound is then applied over the target organs or tissue. With optimal pressure and frequency, these waves induce oscillations of the microbubbles and can eventually lead to cavitation of the microbubble. The energy released through the cavitation process releases the DNA, and induces pores on the membrane of cells near the microbubbles. The DNA then enters these cells, resulting

in gene transfection. The goal of this project was to deliver plasmids to the placental cells (trophoblasts) of C57BL/6 mice.

A significant tool in electrical engineering is the development of impedance spectroscopy (IS). This technique generates an electrical signal which is swept over a preset frequency range to identify certain characteristics of the target substrate, device, or object. The goal of IS is to characterize the target material, medium, or object with a specific impedance and phase measurement over the swept frequency range. This characterization of impedances then can be compared to specific properties of the target. Here we discuss the application of IS to correlate the varying impedance measurement to the developmental changes of different organisms. These two projects are detailed in this work and they cover just a small part of the early stages of development in mice and *Artemia*. Sonoporation was used in experiments for pregnant mice, specifically to deliver genes to trophoblasts and IS was used to characterize the condition of *Artemia* cysts until their hatching. The last chapter in this thesis summarizes the two projects and concludes with some future improvements and ideas.

CHAPTER 2 GENE DELIVERY WITH THE SONOPORATION TECHNIQUE

In America one in three adults are obese, and one in 20 have extreme obesity [6]. A study conducted by the National Institute of Diabetes and Digestive and Kidney Diseases (NIDDK) from 1962 to 2010 has found that there has been an increase of people who are either obese or have extreme obesity (Fig. 2.1) [6].

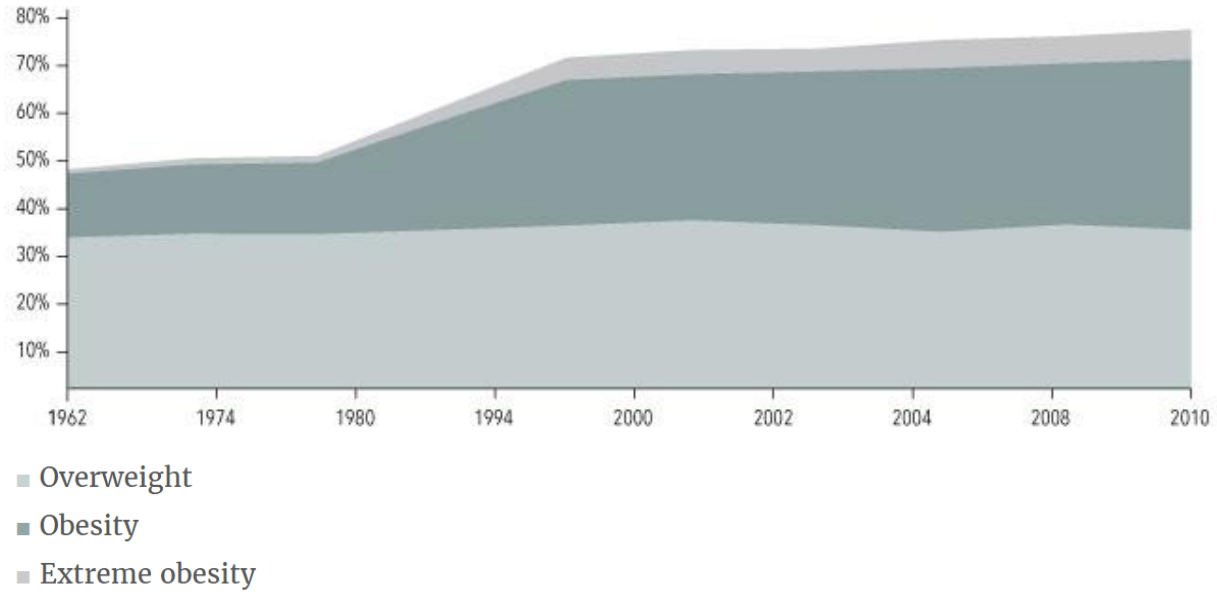

Figure 2.1: The percentage of the US population that is overweight, obese or extremely obese. The prevalence of obesity and extreme obesity has been increasing since 1962. Figure reproduced from ref. [6].

Approximately 38.25% of women between the ages of 20 to 59 were obese in America from 2011 to 2014, according to the US Department of Health and Human Services [7]. If these women are pregnant, they present increased health risks not only to themselves, but to their babies as well. Examples of these health risks include pregnancy loss, birth defects, stillbirth, and fetal overgrowth [8]. Furthermore, children born to obese mothers are at higher risk of developing diabetes, obesity, and heart disease [9].

Controlling the amount of nutrients a fetus receives during gestation can counter the negative effects of maternal obesity. One way to achieve this goal is to regulate glucose transport within the placenta. There are some potential treatment options for obese mothers such as diet and exercise [10], bariatric surgery [11], and viral gene delivery [12]. In this thesis, a non-viral approach, utilizing ultrasound, is explored for gene therapy to regulate glucose transport in the placentas of obese mothers.

2.1 Animal Model

Glucose has been found to be one of the most significant nutrients necessary for fetal development [13]. It is well known that in mammals the mother delivers nutrients via the blood stream to the fetus; and the intermediary step in this nutrient transfer process is the placenta [13]. If a fetus receives too many nutrients, from his or her overweight or obese mother, it may lead to fetal overgrowth. This may not only lead to complications at delivery but can also be particularly perilous for the newborn as she/he is more likely to develop Type 2 diabetes later in life. Therefore, there exists the challenge of regulating the glucose transporters within the placenta. This can be achieved using gene transfection. There are mouse models for obesity during pregnancy; this research focuses on pregnant mice and investigates how to efficiently deliver transgenes to the placenta of mice.

Mice are used in research as their genome shares many similarities with the human genome, they are easy to work with, and are relatively inexpensive [14]. Of the 4,000 studied genes in mice and humans, less than 10 are uniquely found in one but not the other [15]. Thus, mice are a suitable animal model for testing ultrasound for gene delivery.

There are many different breeds and strains of mice; the most commonly used is the C57BL/6 strain [16]. Fig. 2.2a depicts a Swiss Webster (SW) mouse, while Fig. 2.2b shows a C57BL/6 mouse. The C57BL/6 has black fur whereas SW mice have a white coat. These two types of mice were used during this research project, and it is very obvious to tell them apart from their previously noted physical characteristics.

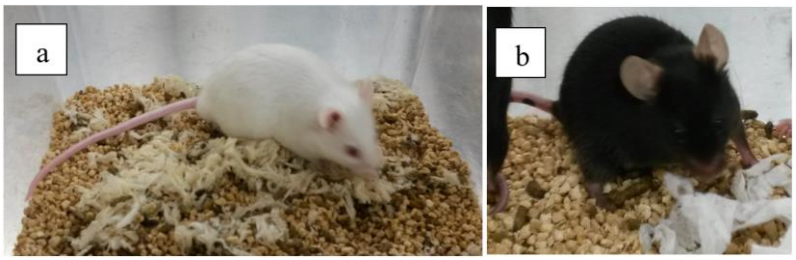

Figure 2.2: The SW mouse (a) and C57BL/6 mouse (b). SW are naturally bigger than the C57BL/6, and have much different physical characteristics.

Mice were bred at approximately three months of age, with two female mice per one male mouse. Placental experiments were then conducted when the mice reached day 14 of their pregnancy, or two weeks after initially breeding them. A mouse placenta has a diameter roughly equivalent to that of a dime, varying in size between 4 mm and 8 mm from 10 days to 18 days of gestation [17].

2.2 ULTRASOUND

To facilitate gene transfection, ultrasonic energy is used. Ultrasound describes acoustic waves with frequencies above 20 kHz (Fig. 2.3).

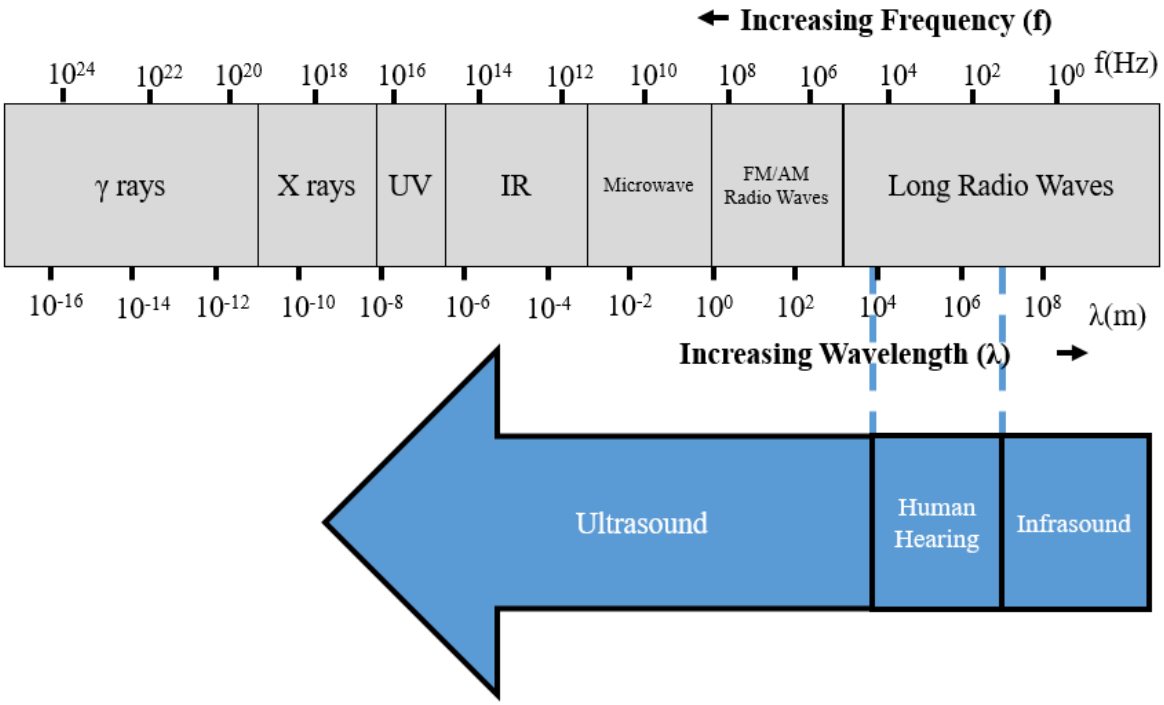

Figure 2.3: Relevant acoustic parameters for human hearing. Infrasound are acoustic frequencies below 20 Hz, human hearing are frequencies between 20 Hz to 20 kHz, and ultrasound are frequencies above 20 kHz.

In non-destructive testing ultrasound is used to detect and identify abnormalities within uniform solids [18]. This is carried out by placing an ultrasound transducer over the target object, applying ultrasound pulses, and detecting the reflected ultrasound. Abnormalities such as cracks in the material cause mechanical impedance mismatches, and can thus be detected. Ultrasound is widely used in the medical profession today as an imaging tool [19]. Pregnant mothers commonly undergo routine ultrasonic imaging to visualize the development of their baby.

The practice of using ultrasound for imaging within a body is called ultrasonography. In ultrasonography sometimes contrast agents are used to assist in imaging of organs, arteries, or tissues of interest. Initially discovered in the 1960's by Dr. Charles Joiner, microbubbles were found to have been beneficial in providing a transient ultrasound signal [20]. This means that the gradient between received acoustic signals from the microbubbles, and the interior organs and/or

tissues was large and improved the quality of the ultrasound image. There are several pieces of equipment in ultrasonography which will be discussed, one of the most important being the ultrasound transducer.

A transducer is a device which converts one form of energy to another. In ultrasonography, a transducer converts electricity to mechanical motion (Fig. 2.4). This process is achieved using piezoelectric material.

Figure 2.4: An ultrasound transducer manufactured by General Electric (GE). This transducer has a 6.35-mm-diameter face, and is approximately 76.2 mm long. The black tape on this transducer is to prevent any water leakage during the ultrasound characterization process.

Piezoelectric materials have been used for a variety of applications in sensors, oscillators, micro-electromechanical systems (MEMS), filters, and actuators. These materials have crystal structures that induce an electric potential when a force is applied, and that conversely physically deform when an electric potential is applied to them. The resultant current from an applied force is given by Eq. (2.1) where q is the displacement current (C), k is the piezoelectric constant (C/N), and f is the applied force (N). The induced current is therefore directly proportional to the applied force, and k is a material property [21].

$$q = kf \tag{2.1}$$

By comparing a piezoelectric to an equivalent parallel plate capacitor, the voltage of a piezoelectric can be mathematically represented by Eq. (2.2), where *v* is the induced voltage, *x* is the distance between the parallel plates used to measure the voltage, *C* is the capacitance, ε_0 is the permittivity of free space, ε_r is the permittivity of the target material, and *A* is the area of overlap between the two parallel plates [21].

$$v = \frac{kf}{C} = \frac{kfx}{\varepsilon_0 \varepsilon_r A} \tag{2.2}$$

Eq. (2.2) shows that a voltage across a piezoelectric material can cause a material deformation *x*. Although these equations give a fundamental view of the induced current and voltage in piezoelectric materials, to accurately depict the induced current and voltage a matrix-based approach must be analyzed. For applications in the real world this will require simulation tools such as COMSOL™ and Matlab™. A mathematical relationship for these matrix calculations are not discussed in this paper but can be found in [19].

In addition to the applied current and voltage, the operating environment of the transducer is important to consider. For example, a transducer used in air will behave differently than a transducer immersed in water, due to the differences in the impedances of the environment. In acoustics, there are four key types of impedance, which are defined in [22]:

1. Characteristic Impedance Z_0 $(\frac{Ns}{m^3})$
2. Sound Field Impedance (or Specific Acoustic Impedance) Z_S $(\frac{Ns}{m^3})$
3. Acoustical Impedance Z_A $(\frac{Ns}{m^5})$

4. and Mechanical Impedance Z_{MI} ($\frac{Ns}{m}$).

Furthermore, the characteristic impedance can be found as a product of ρ, the density of the medium, and *c*, the speed of sound, $Z_0 = \rho_0 c_0$. The sound field impedance for a plane wave can then be shown by Eq. (2.3) and Eq. (2.4) [22]:

$$\frac{\underline{p}_+}{\underline{u}_{x+}} = \rho_0 c_0 = Z_0 \tag{2.3}$$

$$\frac{\underline{p}_-}{\underline{u}_{x-}} = -\rho_0 c_0 = -Z_0 \tag{2.4}$$

In electromagnetic theory, the transmission $\hat{T}$ and reflection coefficient $\hat{R}$ are given by Eq. (2.5) and (2.6) where $1 + \hat{R} = \hat{T}$ [23].

$$\hat{T} = \frac{2\hat{\eta}_2}{\hat{\eta}_1 + \hat{\eta}_2} \tag{2.5}$$

$$\hat{R} = \frac{\hat{\eta}_2 - \hat{\eta}_1}{\hat{\eta}_1 + \hat{\eta}_2} \tag{2.6}$$

The transmission and reflection coefficients are similar in the case of acoustics if the intrinsic impedance term η is replaced with the acoustic equivalent impedance Z_0. The boundary condition at the point of intersection between two different materials is that the wave velocity $\underline{u}$ as well as pressure $\underline{p}$ must be continuous, or $\underline{p}_1 = \underline{p}_2$ and $\underline{u}_1 = \underline{u}_2$ at x = 0. This fact can be leveraged to find the respective transmission and reflection coefficient for a pressure front as shown in Eq. (2.7) and Eq. (2.8) [22].

$$\hat{T} = \frac{2\underline{Z}_2}{\underline{Z}_1 + \underline{Z}_2} \tag{2.7}$$

$$\hat{R} = \frac{\underline{Z}_2 - \underline{Z}_1}{\underline{Z}_1 + \underline{Z}_2} \tag{2.8}$$

As previously mentioned, ultrasound transducers must be carefully designed to not reflect the generated acoustic wave. Therefore, to achieve the greatest transmission the impedance of the transducer must be matched to the target medium. If the impedances are not matched, then an attenuated signal is either received or transmitted from the transducer, which could potentially be below the threshold of ambient noise.

Noise is an environmental condition which is inescapable and manifests itself from the random processes of nature. Noise may arise from thermal fluctuations, material defects, and other environmental interference (e.g. power lines). To quantify the effect of noise, the signal-to-noise ratio is commonly used. In terms of acoustics, this can be shown in Eq. (2.9) where S_C is the combined noise and desired signal and S_N is the noise only.

$$SNR = \frac{S_C - S_N}{S_N} \tag{2.9}$$

Most times in controlled environments, such as a lab, noise can be either controlled or accurately accounted for through various means depending on the application and/or experiment.

Attenuation is another key factor in ultrasound. Sound intensity in a spherical wave decreases by a factor of $1/r^2$ and sound pressure decreases by a factor of 1/r, where r is the distance from a point source, and this is known as geometrical attenuation. In addition, as an acoustic wave propagates through space it experiences loss due a variety of factors which transform the acoustic wave into heat energy, which is a process known as absorption [22]. The resulting intensity of the wave is therefore proportional to an exponentially decaying term, which is shown in Eq. (2.10) where I(x) is the intensity of the wave propagating across a distance x, and $\boldsymbol{\alpha}$ is the attenuation coefficient [22].

$$I(x) \propto e^{-\alpha x/2} \tag{2.10}$$

The attenuation coefficient $\boldsymbol{\alpha}$ is defined for varying media and/or substrates, and will be shown later in this paper to have some value when quantifying the health risks for ultrasound-related experiments.

Directivity is a measure of how focused an ultrasound wave is. For example, a simple point source has a directivity of 1 as it generates a sound wave in a spherical shape. On the other hand, a source which concentrates the output to 1/8 of a sphere will have a directivity factor of 8. This is shown in Eq. (2.11) where W is the sound power, and Q is the directivity factor. There are applications where directive sources are preferred, e.g. high-intensity focused ultrasound or headphones, or where less directive sources are preferred, e.g. sonar or music speakers.

$$I = \frac{W \cdot Q}{4\pi r^2} \tag{2.11}$$

An optimal design of a transducer for ultrasonography is typically designed and built with a characteristic impedance value roughly equivalent to that of water. This is because the characteristic impedance of blood and ultrasound gel, which is generally applied to a person's skin to reduce losses, is roughly equivalent to that of water. Also, attenuation must be considered to accurately gauge the signal which will be transmitted from the ultrasound transducer. Table 2.1 summarizes several selected acoustic properties of human tissues and materials which are taken from [24]. In Table 2.1, $\boldsymbol{\alpha}$ refers to the attenuation coefficient.

Table 2.1: A summary of selected acoustic parameters from [24].

Tissue or Material	**Density** $(\frac{g}{cm^3})$	**Speed of Sound** $(\frac{m}{sec})$	**Specific Acoustic Impedance** $(\frac{N}{m^3})$	α $(\frac{db}{cm})$ **@f MHz**	$\alpha = a \cdot f^b$	
					a $(\frac{db}{cm \cdot MHz})$	b
Water	1	1480	1.48	-	0.002	2
Blood	1.055	1575	1.66	-	0.15	1.21
Fat	0.95	1450	1.38	-	1	1
Liver	1.06	1590	1.69	-	0.9	1.1
Kidney	1.05	1570	1.65	-	1	1
Heart	1.045	1570	1.64	2 @ 1 MHz	-	-
Axial Bone (Longitudinal Waves)	1.9	4080	7.75	2-15 @ 0.2-1 MHz	-	-
Axial Bone (Transverse/Shear Wave)	1.9	2800	5.32	2-15 @ 0.2-1 MHz	-	-

Mechanical Index (MI) and Thermal Index (TI) are terms in ultrasonography which are used to identify the safe levels of ultrasound use. The MI is based on a relationship between the mechanical or shear stress introduced to the target host from the output pressure waves of the ultrasound transducer whereas the TI observes the relationship between heat generation and the output power from the ultrasound transducer. There are also other methods which the output energy of the transducer can convert to such as movement of internal fluids or even cavitation, and these are undesirable side effects in a given experiment [25]. Eq. (2.12) shows the MI as the ratio between the peak negative pressure p^- and root of the applied frequency f_c. Eq. (2.13) then shows the TI as the ratio between the output power W and the power it takes to raise the tissue temperature by 1˚C W_{deg} [19].

$$MI = \frac{p^-}{\sqrt{f_c}} \tag{2.12}$$

$$TI = \frac{W}{W_{deg}} \tag{2.13}$$

These parameters establish a basis for which the potential negative effects of ultrasound due to pressure, frequency, and output power are often quantified. A value of 0.7 for the MI is defined as the threshold for inertial cavitation, and although it has been suggested that tissue damage correlates to the applied frequency experimental evidence has yet to prove this [26]. The TI can be applied to three different types of tissue models: soft-tissue thermal index (TIS), bone-at-focus thermal index (TIB), and the cranial-bone thermal index (TIC) [26]. The use of TIS, TIB, and TIC determine the value of W_{deg} in Eq. (2.13), and the derating factor corresponding to an allowable pressure input. TIB assumes half the input power is absorbed, TIC assumes that a majority of the ultrasonic energy is reflected (e.g. 0 transmitted power), and TIS is then given a derating factor of 0.3 dB $cm^{-1}MHz^{-1}$.

There are some ultrasonography systems which provide on screen values for the MI and TI, but they should not be used to quantitatively determine the exposure parameters for an experiment. Instead the transducers should be individually characterized, a process which we discuss later. From the characterization scheme, a more accurate calculation for the MI and TI can then be processed to ensure a more reliable and safe use of the ultrasound equipment.

The near-field distance is identified as a place where the waves generated by the ultrasound transducer are at a peak value, however this parameter changes depending on the mode of operation and whether a pulsed wave (PW) or continuous wave (CW) is used. Therefore, this will not be discussed in this paper and the reader is directed to [19].

2.3 ULTRASOUND CHARACTERIZATION/OPTIMIZATION

Prior to beginning the sonoporation experiments a characterization for the ultrasound equipment is necessary. This is done to ensure that a safe, efficient, and reliable experiment can be performed. The following equipment was needed for the ultrasound characterization process that was performed in this study:

1. 5 metal pipes (roughly 9.5 mm diameter)
2. 2 knockout boxes
3. 1 five-sided acrylic tank (no top)
    a. 9.525 mm thick walls
    b. 25.4 cm (width) by 25.4 cm (height) 40.64 cm (length)
4. Arbitrary waveform generator (Tektronix)
5. Digital oscilloscope
6. RF amplifier
7. Hydrophone (Onda)
8. Polytetrafluoroethylene (PTFE) tape
9. Manual handheld calipers
10. Adhesive velcro strips
11. Electrical tape
12. Laptop with Matlab
13. Ultrasound transducers (focused and unfocused)

The setup for the characterization process is illustrated in Figure 2.5. The blue area indicates that water was added to the plexiglass tank to fully submerse both the ultrasound

transducer and the hydrophone. Specific ultrasound parameters are input into the arbitrary waveform generator (e.g. pulse duration, pulse repetition period, input voltage). The amplifier connects to the waveform generator to increase the overall power output to finally drive the ultrasound transducer. Although the specification of the amplifier states a 53-dB gain (gain of approximately 450) the characterization showed that the amplifier had a saturated gain of approximately 400. Although the amplifier was not exactly operating as stated by the manufacturer's specifications, the amplifier did have a stable gain of 400 across a range of voltage inputs (from 50 mVpp to 200 mVpp with a step increment of 10 mVpp) so it was deemed usable for this study.

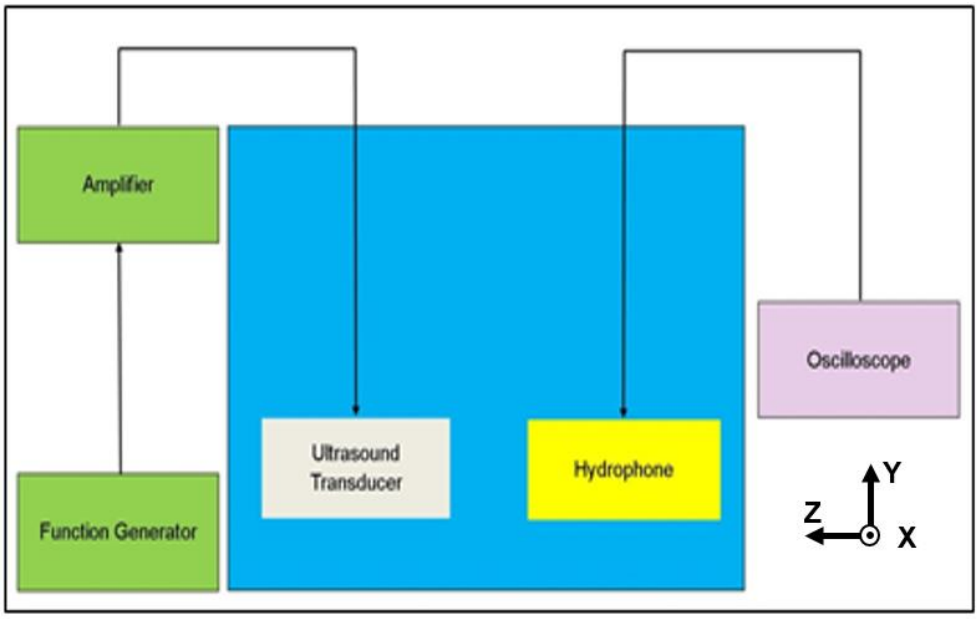

Figure 2.5: Ultrasound characterization setup. A function generator connects to an amplifier, which generates enough power to drive the transducer. A hydrophone converts the mechanical impulses to a voltage which is read on the oscilloscope.

There were three main ultrasound transducers that were used in this study, and all of them were immersion based. Two unfocused transducers were used, one from GE (part number 113-221-340) and the other from Olympus (I4-0108-S-SU U8420054 Olympus). The major difference

in these transducers is that the GE model has a face diameter of 12.7 mm and the Olympus transducer has a face diameter of 25.4 mm. Therefore, it takes much more power to not only drive the Olympus unfocused transducer but to achieve the same pressure output as the GE transducer due to the large difference in piezo material that is subject to the input voltage signal sweeps. The third transducer which was used in this study was a focused Olympus transducer. The voltage necessary to achieve the same pressure output is much less than either unfocused transducer due to the focusing of the ultrasound pulses, however this is a trade-off in terms of the area which is impacted by this pressure output. The focused and unfocused transducers are discussed in more detail later in this section.

The hydrophone receives incoming acoustic pulses and converts this mechanical energy into an electric signal. The sensitivity of the hydrophone used in this study at 1 MHz was -281 dB relative to 1 $\frac{V}{\mu Pa}$. This value was calculated to be 89 $\frac{mV}{MPa}$, which was used in the Matlab code to acquire data points from the digital oscilloscope. Using this sensitivity, and knowing that the oscilloscope will provide a voltage reading from the hydrophone, the pressure input can be found. Eq. (2.15) details an equation which summarizes this relationship:

$$P_{Hydrphone} = \frac{Voltage}{Sensitivity} \tag{2.15}$$

For example, if the input voltage was 0.89 V then the resulting pressure could be calculated as follows:

$$P_H = \frac{890\ mV}{89\frac{mV}{MPa}} = 10\ MPa$$

In the ultrasound transducer characterization setup, an oscilloscope is connected directly to the hydrophone. A laptop was then connected to the oscilloscope via a USB cord, and a Matlab

executable file was run to acquire the data points from the oscilloscope and stored in an excel file on the laptop. Details of the Matlab file is explained in detail later in this section.

The characterization setup was custom-built, and used sliding cameras on metal pipes. Metal pipes were chosen over PVC because they are more durable and were cheaper. The knockout boxes, PTFE tape, and the metal pipes were purchased at a local store for under $30. The largest cost of the initial setup was the acrylic tank, which cost about $300.

The pipes were cut to an appropriate size using a hack saw, and indelible ink was used to mark tick marks on the pipes, spaced 2.5 mm apart. This system was used for characterization of the various ultrasound transducers during the two-year duration of this project, and will be used by researchers in this lab in the future. Figure 2.6 shows the final ultrasound characterization setup.

Several transducers were purchased through Olympus and GE which varied in size. One focused transducer was used in the present study and the rest were unfocused transducers. A focused transducer has a concave face to focus the emitted ultrasound pulses at a specific distance from the transducer, based on the curvature of the concavity. These pulses are meant to intersect at a point, meaning that the total volume of intersection for these pulses is intended to be as small as possible.

The initial characterization process necessitated the use of a characterization map, or a coordinate system with detailed ultrasound parameters under investigation for a specific transducer. Over the course of the study the characterization process improved, and customized studies were performed at specific coordinates and ultrasound parameters. Therefore, for characterization there were two major schemes: a full characterization or a custom characterization.

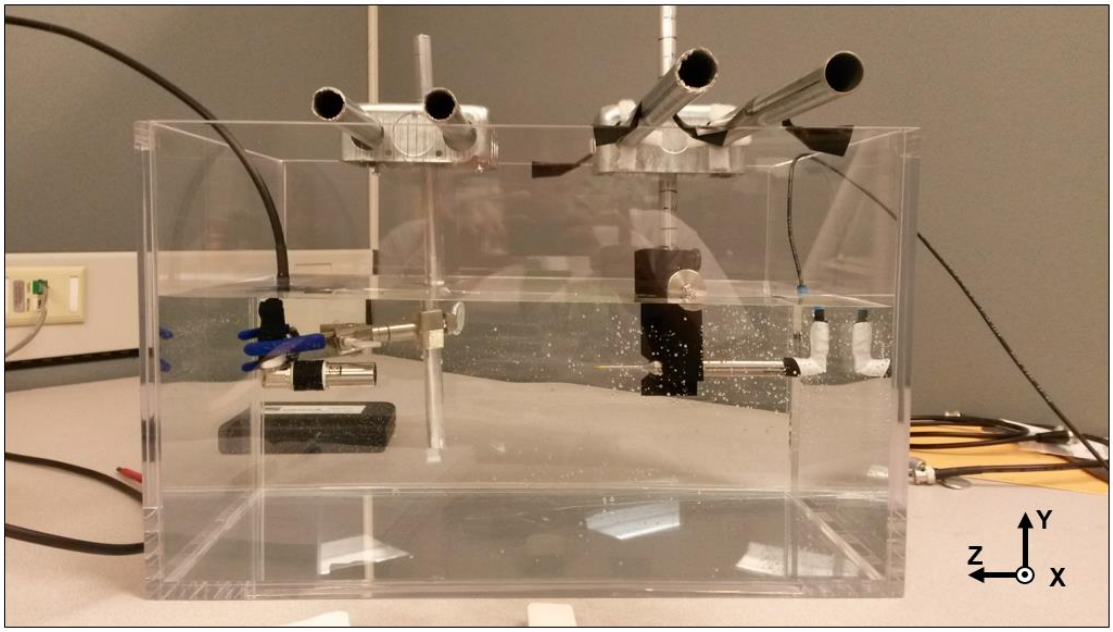

Figure 2.6: The realized ultrasound characterization setup. This characterization process was less expensive than sending the transducers to be calibrated at a certified lab or company.

It was empirically determined for the Olympus focused ultrasound transducer that the focal point was approximately 15.24 mm away from the transducer face, and had a cylindrical convergence profile with a radius of 2.5 mm and length of 2.5 mm. The unfocused transducers create ultrasound pulses which behave similarly to the equations that were presented earlier in this chapter.

An advantage of focused ultrasound is that the isolation of ultrasound pulses is possible but at the same time a complication that is introduced is the complexity of the setup increases as the positioning of the transducer becomes paramount to ensuring a successful experiment. Conversely the advantage of unfocused ultrasound is that the experiment setup process is much simpler but all tissues and organs beneath the face of the transducer are subject to the ultrasound pulse energy.

The Matlab file which was programmed to connect to the oscilloscope, acquire data points from the ultrasound pulses, and then store and save them to a Microsoft Excel file, became an essential part to working with the ultrasound setup. By implementing a Matlab executable, the ultrasound characterization process became streamlined and easy enough for everyone to operate, if given brief instructions.

Over time the peak pressure output of the ultrasound transducer decayed. This effect was apparent during CW modes of operation during characterization and was minimized during PW modes of operation. The underlying reason is that the piezo material of the transducer may have been experiencing over saturation, and in some initial experiments this led to the degrading and failure of some of the transducers. Only PW modes of operation were used in the characterization process of the ultrasound transducers to reduce the effects from oversaturation of the piezoelectric material. Matlab code was used to obtain 2500 sample points from the oscilloscope for several different times during the interrogation of the ultrasound transducer. The time points in which 2500 sample points were taken were at 1.7, 3.4, 5.1, 6.8, 8.5, 10.2, and 11.9 seconds after the ultrasound transducer was initially excited for one characterization. The spacing between time points was determined by using the *tic toc* command in Matlab which records how long it takes to run particular instances of code, depending on the spacing between *tic* and *toc*. It took approximately 1.7 seconds to run the entirety of the Matlab code, which increased to 11.9 after the 7 iterations. The oscilloscope is called within the Matlab code via the USB port, and data points were saved to two separate matrices, h and k. The raw data from the experiment lie within the h matrix whereas k contains information regarding the oscilloscope parameters (e.g. the time between two sample points). The next lines searches for the peak and the minimum voltage values, and converts this to a pressure value using Eq. (2.15). The benefit of using the Matlab executable

is that both the raw data, and the pressure converted data can be stored simultaneously within approximately 15 seconds (11.9 seconds to run the code and a few extra seconds to finally save the excel file). The code is provided in Appendix A.

The first transducer to be characterized was the Olympus unfocused transducer. All characterizations started with the center coordinate on the characterization map, and moved on the X and Z axis with a resolution of 2.5 mm (the tick marks on the metal pipes). The largest characterization map for this transducer was a 5 by 5 array with voltages between 50 mVpp and 850 mVpp with 50 step increments. There were two unfocused Olympus transducers, so both were characterized consecutively. The characterization of the Olympus transducer showed that a majority of the input voltages did not produce an output greater than or equal to 1 MPa, which meant that little to no successful sonoporation could actually be conducted. Thus, the Olympus unfocused transducer was not used for sonoporation; instead the Olympus focused transducer and the GE transducer were used. The Olympus transducer outputs are summarized in Table 2.2.

Next, a characterization map for the GE unfocused transducer was performed and is shown in Figure 2.7. The imagesc tool was used in Matlab to color the changing pressure value as a function of time, and as can be seen the pressure decreases over time. The output pressures are then displayed in Table 2.3 for both the GE 1 and GE 2 transducers which were used in this study.

It was also discovered that the unfocused transducers from both GE and Olympus could be characterized by the peak pressure, which was usually around the center of the transducer face. From this finding, it was determined that for routine checks with the transducer a custom characterization can be performed which involved finding the peak pressure point in relation to the transducer face and doing an input sweep from a low to high voltage. The full characterization

map is therefore only necessary every six months, or when the peak pressure is significantly different than previously recorded. This is an important finding because it enabled the current study to quickly characterize purchased transducers and implement them in the sonoporation experiments.

Table 2.2: Testing points for the Olympus focused and unfocused transducer. The induced pressure greatly differs for the focused and unfocused transducer.

Time (s)	Pressure (MPa) with a 650 mVpp Input	
	Olympus Unfocused	Olympus Focused
1.7	0.58	4.58
3.4	0.56	4.40
5.1	0.58	4.85
6.8	0.58	5.48
8.5	0.58	4.85
10.2	0.59	5.48
11.9	0.58	4.94

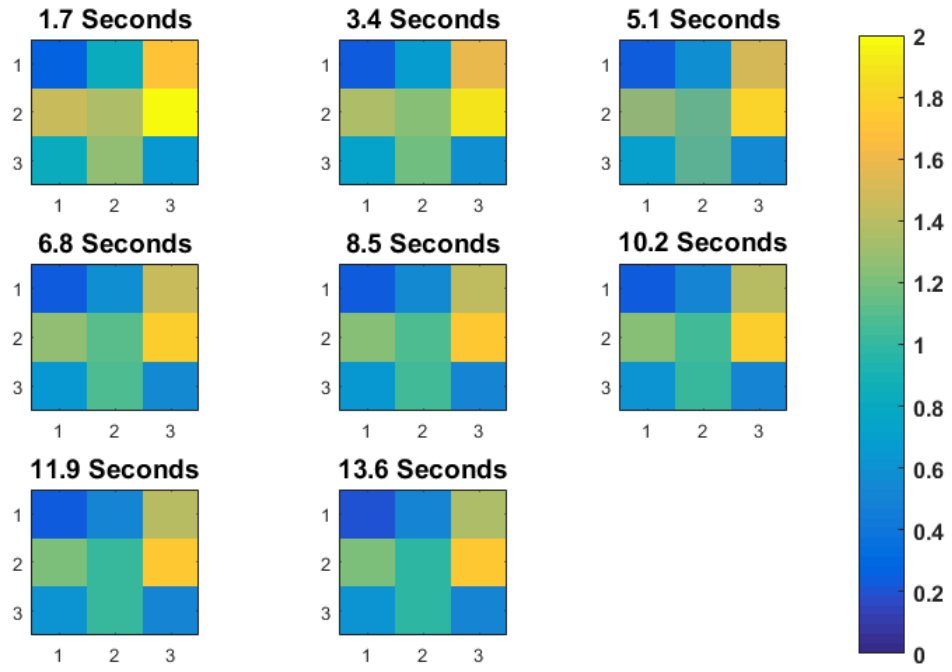

Figure 2.7: Characterization map of GE 1 unfocused transducer plotted using the Matlab imagesc command. Initially the transducer has a transient pressure output, but at 11.9 seconds it reaches a steady-state output.

Table 2.3: Testing points for the GE unfocused transducers. Much like the Olympus unfocused transducers, the GE transducers were found to have similar pressure outputs.

Time (s)	Pressure (MPa) with a 650 mVpp input to the amplifier	
	GE 1	GE 2
1.7	1.71	1.55
3.4	1.66	1.48
5.1	1.59	1.43
6.8	1.57	1.41
8.5	1.55	1.39
10.2	1.53	1.32
11.9	1.50	1.37
13.6	1.50	1.37

After characterization of the ultrasound transducers, the overall aim of gene transfection into cells could be carried out. Microbubbles were used as carriers for plasmids because they could flow through the bloodstream, thus being able to penetrate any organ or tissue within the body that blood is able to. This technique is known as sonoporation.

2.4 SONOPORATION

Sonoporation is the induction of the transient porosity of cells using ultrasound. Sonoporation, to deliver genes to an organ or tissue, uses ultrasound induced cavitation of plasmid coated microbubbles to achieve targeted gene transfection. The use of the sonoporation technique with microbubbles is illustrated in Fig. (2.8). Several processes (e.g. pushing, pulling, jetting, shearing, translation), occurring most likely simultaneously during microbubble cavitation induces gene transfection, and are summarized in [19].

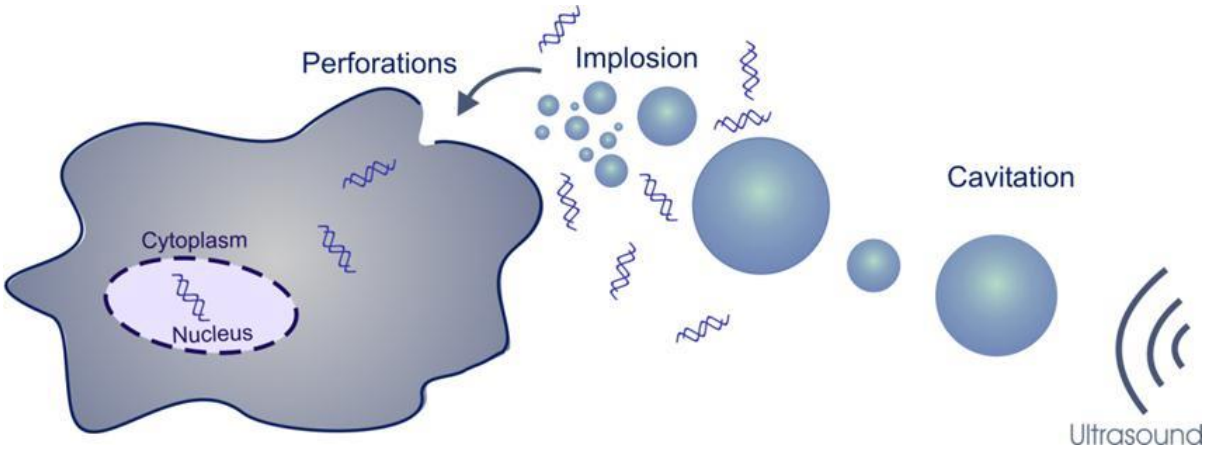

Figure 2.8: The sonoporation technique with microbubbles. As ultrasound pulses are emitted from the transducer, they induce microbubble oscillations. The force from this process leads to pores on the cellular membrane. The plasmids which once coated the microbubbles enter the cell through these pores and gene transfection results. Figure reproduced from ref. [27].

2.5 BUBBLES AND DNA

A plasmid is DNA which has been formed into a circle. Plasmids, also called vectors, can be bioengineered to enable cells to perform specific tasks [28]. Hence these plasmids are used to deliver transgenes by mechanisms such as sonoporation. Another benefit of using plasmids is that they can be rapidly generated using bacteria, which are able to generate a large supply if needed [28].

In the experiments presented here, there were three plasmid types which were used: pGL3, Genie3-GINbb-Ept1 (Ept1), and Genie3-GINbb-TRE3G-LUC-CYP-TRCN0000311403 (Glut1). Table 2.4 highlights the major characteristics of each of these plasmids.

Table 2.4: Key characteristics of the plasmids used in this work.

Plasmid Name	Doxycycline Injection Required	Tissue Specific
pGL3	No	No
Ept1	Yes	No
Glut1	Yes	Yes, placental

All three plasmids were engineered to contain the luciferase assay reporter. Luciferase is an enzyme which converts the substrate luciferin, here delivered by intraperitoneal injection. Bioluminescence is a byproduct of this process, and an example of this is the firefly. To quantify the intensity of this light, as well as the gene delivery effectiveness, an integrated imaging system, known as the In Vivo Imaging System (IVIS) was used. This method allowed for a repeatable, simple, and quick verification of gene delivery.

Doxycycline is commonly used for humans as an antibacterial drug. It is a derivative of tetracycline, and most importantly allows for the activation or de-activation of target genes through the mechanisms known as TET-system [29]. Two plasmids, Ept1 and Glut1, contained the TET-system and required doxycycline to activate the expression of luciferase.

Contrast agents are sometimes used in ultrasonography to improve image quality [20]. These contrast agents increase the backscatter, or the amount of reflections back to the imaging transducer, from blood, allowing imaging of smaller features such as capillaries within the body [24]. The contrast agents can be identified as gas filled microbubbles with an outer layer consisting of a specific material. These microbubbles can also act as more than a contrast agent, as they can also be used for gene delivery.

Microbubbles approximately 1 to 3 μm in diameter were used in this study [30]. A blood vessel is a part of the circulatory system that transports blood, and thereby red blood cells (RBCs) throughout the human body. RBCs vary in size from 6 μm to 8 μm [31], and the similarity of sizes between microbubbles and RBCs allow the microbubbles to the same pathways that RBCs take throughout the body. Examples of blood vessels are capillaries, arteries, and veins. The largest blood vessel in the body is the aorta artery with a diameter of 25 mm, and the smallest blood vessel is the capillary with the smallest diameter of 8 μm [32]. The varying sizes of these blood vessels can drastically impact the flow profile of the RBCs and microbubbles and in turn the amount of pressure that they experience.

The microbubbles used in this study are filled with a gas called octofluoropropane, an inert gas which is heavier than gases found in the atmosphere, a lipid outer shell, and a plasmid construct. As DNA is negatively charged, it adheres to the positively charged lipid shell of the

microbubble through electrostatic forces [33, 34, 35]. These microbubbles are introduced into the bloodstream through cardiac injection, and then cavitation of the microbubble is induced with a targeted ultrasound pulse. For this work, microbubbles were created as shown in Figure 2.9.

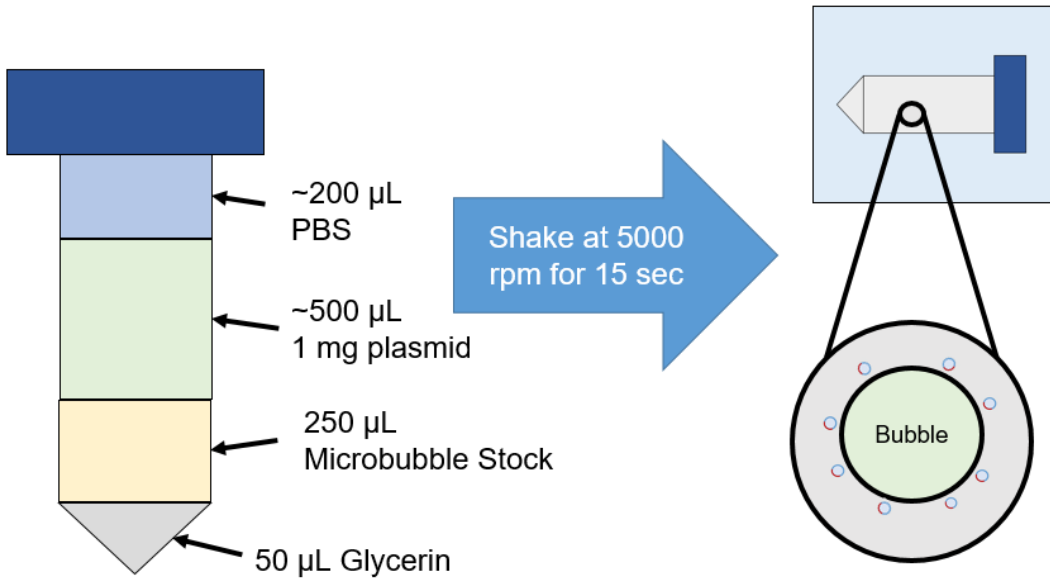

Figure 2.9: A graphic showing the generation of microbubbles. 1 mg of plasmids were used which would typically amount to 500 µL, and the remaining volume would be topped off at 1 mL with phosphate buffered saline (PBS) which typically was 200 µL. The microtube was then vigorously shaken at 5000 revolutions per minute for 15 seconds using a dental amalgamator, and put on ice. This would ensure quality microbubbles for approximately 2 hours. The microbubble is shown to be coated with plasmid constructs.

2.6 Current Sonoporation Research

A recent PubMED search for sonoporation yielded 100 publications. The transducer parameters were extracted from each paper and organized in Table 2.5. These parameters determine the characteristics of the ultrasound used in each experiment and consist of the following: frequency (MHz), mode of operation (pulsed wave, PW, or continuous wave, CW), intensity or peak pressure (W/cm^2 or MPa), pulse repetition rate/period, pulse repetition frequency

(sec or Hz), duty cycle (%), MI, and exposure time (s). In addition to these parameters, the target organ and method of delivery were recorded. The target organ influences the chosen ultrasound parameters and includes the depth and physical characteristics of the organ (e.g. size and orientation relative to a mouse abdomen). The method of delivery was also recorded because the infusion point may impact the sonoporation experiment by affecting the initial pressure experienced by the microbubbles (e.g. the tail vein will induce a larger exterior pressure on the microbubble than a heart injection). In addition, the location of entry for the microbubbles may dictate whether the bubbles are immediately delivered to the target organ or tissue (e.g. direct muscular injection) or must go through the body, into the heart, and finally to the target organ (e.g. tail vein injection to heart to target organ). If the pressure is too large, the microbubbles may rupture and never reach the desired organ. The literature review revealed two common methods of injection: direct and tail vein. Direct injections included injecting microbubbles, via a needle and syringe, into the target organ and then continuing the sonoporation experiment. A tail vein injection relied on intravenously injecting microbubbles through the tail of the mouse. Another method reported was a cardiac injection of microbubbles, followed up with ultrasound to the target organ. This third method involved injecting microbubbles to the left atrium of the heart and then allowing both the blood stream and blood vessels to transport microbubbles to the desired organ where sonoporation was then performed.

Of the 98 manuscripts reviewed, 73 used a frequency in the range 1 of 2 MHz. Thirty-eight papers reported microbubble delivery using the tail vein, 33 papers used direct injections, and the remainder used another type of injection. Seventy-nine publications reported whether they used a CW or PW mode of operation. Of the papers that reported CW or PW operation, 73 (92 %) used only a PW input and 76 (96.2%) used both PW and CW operation. Nineteen papers reported the

ultrasound pulse duration, but there were no patterns in the reported findings. Seventy-two manuscripts indicated either a peak pressure (28 papers) or peak intensity (48 papers) for the ultrasound transducer. A peak pressure from 1 to 2 MPa was reported six times, while 16 studies used less than 1 MPa of pressure, and six reported a pressure above 2 MPa. Thirty-one papers recorded an intensity value from 1 to 2 $\frac{W}{cm^2}$, with 12 reporting less than 1 $\frac{W}{cm^2}$, and 11 reporting more than 2 $\frac{W}{cm^2}$. Of the 48 publications that reported a duty cycle value, which varied greatly, all remained below 50%. The pulse repetition period (PRP) was reported in 40 papers and was under 100 ms in 18 papers, between 100 to 250 ms in 12 papers, and over 250 ms in 11 papers. Most studies (84 papers) reported an exposure time for their experiment. The exposure time in seven papers was less than 1 minute, 54 papers reported an exposure time between 1 and 5 minutes, and 24 papers reported exposure times longer than 5 minutes.

It was unclear whether the method of microbubble injection was a significant factor in determining whether a sonoporation experiment was successful as several delivery routes for the same organs or tissues were described. We noted that a PW mode of operation shows a stronger relationship to a successful sonoporation experiment than both a CW and/or combined CW/PW mode of operation. The peak pressure or intensity output values showed that a lower pressure output yielded a much more successful sonoporation experiment (less than 1 MPa), and the optimal intensity varies from 1 - 2 $\frac{W}{cm^2}$. The PRP was split evenly between 3 groups: below 100 ms, between 100 ms and 250 ms, and above 250 ms. There is no clear indication as to how significant the PRP is to a successful sonoporation experiment. Duty cycle has been shown in these papers to be best below 50%. The exposure time plays a more significant role in a successful sonoporation experiment, and is more likely to be associated with the method of infusing or injecting

microbubbles into the bloodstream. It was reported that longer exposure times were correlated to longer durations for microbubble infusion methods (e.g. intravenous infusion had an exposure time of roughly 31.5 minutes), whereas for quicker microbubble infusions, such as direct injections, the exposure time was seen to be in the 1 to 5-minute range.

In summary, our literature review revealed that the key ultrasound parameters for a successful sonoporation experiment are as follows:

1. A frequency between 1 to 2 MHz
2. PW mode of operation
3. Peak negative pressure of 1 MPa (or less than)
4. Duty cycle less than 50%
5. And an exposure time between 1 to 5 minutes which varies depending on the microbubble infusion duration.

Data from the literature findings are summarized in two different tables, Table 2.5 and Table 2.6.

Table 2.5: Literature search for sonoporation experiments. PNP stands for peak negative pressure and is a parameter commonly associated with characterization of the ultrasound transducer. In this table the target organ or model of study, delivery route for microbubbles, frequency for the transducer, mode of operation (whether continuous or pulsed wave), and pulse duration are recorded.

Reference	Target Organ or Model	Delivery Route	Frequency	Mode (CW/PW)	Pulse Duration
[30]	Liver	Heart	1 MHz	PW	200 μs
[36]	Liver	Heart	1 MHz	PW	100 ms
[37]	Liver	Portal Vein	1.17 MHz	PW	0; 17; 34; 285; 571 μs
[38]	Liver	Portal vein	1.17 MHz	PW	17.1 μs
[39]	Kidney	Inferior vena cava, laparotomy	3 MHz	PW	
[40]	Well plates	Well plates	100 Hz	PW	
[41]	Retinas	Intravitreal injection	1 MHz	PW	20 ms
[42]	Hindlimbs	Tail vein	1 MHz	PW	5 ms; 50 ms
[43]	Brain	Direct injection	1 MHz	PW	10 ms
[44]	In *vitro*	In *vitro*	1 MHz	PW	
[45]	Skin cancer	Jugular vein	1.3 MHz	PW	
[46]	Breast cancer		3 MHz	PW	
[47]	Breast cancer		3 Mhz, 1 Mhz	PW	
[48]	Brain	Direct Injection	14 MHz		
[49]	Heart	Tail vein	1.4 – 4 MHz	PW	
[50]	Murine limb ischemia	Intravenous infusion	1.6 MHz	PW	400 μs
[51]	Squamos cell carcinoma	Jugular vein	1.3 MHz	PW	4 to 6 bursts
[52]	Arthritis	Foot, tail, and back	10 MHz	CW	
[53]	Thigh muscle	Muscular injection	1.4 MHz	PW	100 cycles
[54]	Brain	Tail vein	1.5 MHz	PW	100 to 1000 cycles
[55]	Tumor	Tail vein	1 MHz	PW	
[56]	Skeletal muscle	Intra-arterial injection	1 MHz	CW	
[57]	Skeletal muscle	Intravenous infusion	1.3 MHz		
[58]	Pancreatic islets	Jugular vein	1.3 MHz, 3.6 Mhz	PW	

Reference	Target Organ or Model	Delivery Route	Frequency	Mode (CW/PW)	Pulse Duration
[59]	Tumor	Retroorbital injection	1.5 MHz	PW	
[60]	Skeletal muscle	Tail vein	1 MHz	PW	0.3 ms
[61]	Skeletal muscle	Direct injection	1 MHz	PW	
[62]	Kidney tumor	Tail vein	1 MHz	PW	
[63]	Varying	Subcutaneous	1 MHz	PW	
[64]	Chronic hindlimb ischemia	Intravenous infusion			
[65]	Coronary injury	Tail vein	1 MHz	PW	
[66]	Hindlimb ischemia	Intravenous infusion	1.3 MHz		
[67]	Tumor	Tail vein	1 kHz		
[68]	Tumor	Tail vein	1 MHz	PW	
[69]	Tumor	Tail vein	1 MHz	PW	
[70]	Myocardial infarcation	Tail vein	8 MHz	PW	1 burst
[71]	Cardiac gene transfer	Jugular vein	1.3 MHz		
[72]	Tibialis muscle, skin, and kidney	Direct, intradermal and intrarenal-parenchymal injection	2 MHz	PW	
[73]	Liver, spleen, lung, kidney, heart	Tail vein	1.045 MHz	PW	
[74]	Cardiac	Direct injection			
[75]	Cardiac	Intravenous infusion	1.3 MHz, 3.6 MHz	PW	
[76]	Liver, skeletal muscle, pancreas	Jugular vein	1.3 MHz, 3.6 MHz	PW	
[77]	Myocardium	Jugular vein	1.3 MHz, 3.6 MHz	PW	
[78]	Cardiac	Jugular vein	1.3 MHz, 3.6 Mhz	PW	
[79]	Video intensity study	Aortic root catheter	2 MHz, 4 MHz, 6 MHz	Both	Varying
[80]	Tumor	Femoral artery	1 MHz	PW	
[81]	Hindlimb ischemia	Tail vein	1 MHz	PW	

Reference	Target Organ or Model	Delivery Route	Frequency	Mode (CW/PW)	Pulse Duration
[82]	Cardiac microbubble desctruction	Right jugular vein	1.3 MHz	PW	
[83]	Myocardial gene transfer	Infusion via left heart ventricle	1.3 MHz, 3.6 MHz	PW	
[84]	Mesenteric vasculature gene delivery	Intravenous bolus retroorbital injection	1 MHz	PW	
[85]	Squamos cell carcinoma	Jugular vein	1.3 MHz		
[86]	Liver	Tail vein	1 MHz	PW	33 μs
[87]	Liver tumor	Tail vein	5 to 12 MHz	PW	
[88]	Breast cancer		1 MHz, 10 MHz		
[89]	In *vitro* endothelial cell study		1 MHz		500 μs; 1 ms; 2 ms; 5 ms; 10 ms; 20 ms; 50 ms
[90]	Skeletal muscle	Direct injection	1 MHz	Both	
[91]	Prostate cancer	Tail vein	5 to 12 MHz		
[92]	Colon cancer	Tail vein	1.8 MHz	PW	Various
[93]	Lymph node tumors	Tail vein	970 kHz	CW	200 pulses
[94]	Liver	Tail vein	1.54 MHz	PW	1.6 μs (2.5 cycles)
[95]	Head and neck cancer	Subcutaneously injected	1 MHz		
[96]	Salivary gland	Submandibular duct cannulation	1 MHz	PW	
[97]	Kidney tumor	Left renal artery catheter	5 to 12 MHz		
[98]	Kidney	Tail vein	1 MHz		
[99]	Malignant ascite	Intraperitoneal injection	1.056 MHz	PW	
[100]	Lymph node tumor	Tail vein	1 MHz	PW	200 pulses
[101]	Liver	Direct injection	1.1 MHz	PW	20 cycles
[102]	Tumor	Direct injection	2.069 MHz	PW	
[103]	Oral tumor	Intraperitoneal injection	1 MHz	PW	

Reference	Target Organ or Model	Delivery Route	Frequency	Mode (CW/PW)	Pulse Duration
[104]	Arthritis	Direct injection	3 MHz	PW	
[105]	Ectopic and orthotopic models		1 MHz	Both	
[106]	Tumor		3 to 9 MHz	PW	2.42 ms
[107]	Adenocarcinoma	Intramuscular injection	1 MHz	PW	
[108]	Pancreatic cancer	Intravenous infusion	1.3 to 2.4 MHz	PW	0.21 ms
[109]	Muscle	Intramuscular injection	1 MHz	PW	
[110]	Tumor	Intramuscular injection	1 MHz	PW	
[111]	Ciliary muscle	Intramuscular injection	1 MHz	PW	5 ms
[112]	Peritoneal macrophages	Intraperitoneal injection	2.5 MHz		
[113]	Tumor	Tail vein	28 kHz; 3 MHz		
[114]	Melanoma	Direct injection	1.011 MHz	PW	
[115]	Skeletal muscle	Intramuscular injection	1 MHz	PW	
[116]	Skeletal muscle	Intramuscular injection	973.65 Hz	PW	
[117]	Tumor	Intraperitoneal injection	1 MHz	PW	
[118]	Lung	Nasal instillation	30.5 to 35.5 Hz	PW	
[119]	Tumor and muscle	Direct injections	1 MHz	PW	
[120]	Parotid	Intraperitoneal injection	1 MHz	PW	
[121]	Hepatic cancer	Direct injection	1 MHz	PW	
[122]	Femoral artery		1 MHz	PW	
[123]	Osteogenesis	Intramuscular injection	1 MHz	PW	
[124]	Joint tiissue	Direct injection	3 MHz	PW	
[125]	Gingival squamous carcinoma	Direct injection	1MHz	PW	
[126]	Heart	Intercostal muscle and tail vein	1 MHz	PW	
[127]	Tumor	Intra-arterial			

Reference	Target Organ or Model	Delivery Route	Frequency	Mode (CW/PW)	Pulse Duration
[128]	Reproductive system	Direct ovary injection		PW	
[129]	Vein graft	Intravenous infusion	1 MHz	PW	
[130]	Hepatocellular carcinoma	Direct injection	1 MHz	PW	
[131]	Dental pulp	Direct injection	1 MHz	PW	
[132]	Muscle	Intramuscular injection	1 MHz	PW	

Table 2.6: Summary of the PubMED literature search on sonoporation. The intensity/pressure of the transducer, pulse repetition period (PRP) or pulse repetition frequency (PRF), duty cycle, MI, and exposure time are tabulated.

Reference	Intensity/Peak Pressure	PRP/PRF	Duty Cycle	MI	Exposure Time
[30]	1.3 MPa (PNP)	10 Hz			5 min
[36]		100 ms for 20 cycles		1.3 to 1.5	5 min
[37]	0; 4.3 Mpa	0 Hz; 3 Hz; 50 Hz	0%; 0.09%; 0.17%; 0.09%; 0.17%		
[38]	4.5 Mpa	50 Hz			
[39]			50%		1 min
[40]	$1\ \frac{W}{cm^2}$		20%		1 min
[41]		100 Hz	50%		5 min
[42]	1.25 MPa (PNP)	30 sec			8.5 min; 16.5 min
[43]	In *vitro* 0.5 MPa (PNP); In *vivo* 0.7 MPa (PNP)	200 ms	5%		1 min
[44]		10 ms	10%, 20%, 30%		40 sec, 50 sec, 60 sec
[45]				1.6 MI	30 min
[46]	In *vivo* 0.24 MPa	In *vitro* 1 Hz, 1.2 Hz, 1.4 Hz, 1.7 Hz, 2 Hz, 2.5 Hz, 4 Hz, 10 Hz; In *vivo* 4 Hz	50%		In *vivo* 2 min
[47]	0.28 MPa; 0.15 MPa	4 Hz; 1 Hz	50%; 12%	0.18; 0.11	2 min; 1 min
[48]					10 sec (repeated 3 times)
[49]				1.3	20 min
[50]		5 sec		0.6; 1.3; 2.4	
[51]		1.5 to 2.5 sec		1.6	30 min
[52]				1.3	10 min
[53]	200 kPa	540 Hz			0.5 to 10 min
[54]	225 to 600 kPa	5 Hz			1 min

Reference	Intensity/Peak Pressure	PRP/PRF	Duty Cycle	MI	Exposure Time
[55]	$2\ \frac{W}{cm^2}$	50%			5 min
[56]	0.32 and 0.41 MPa (PNP)				3 min
[57]	2.1 MPa (PNP)	5 sec			
[58]	Triggered at 80 ms after peak of R wave. 4 frames per 4 cardiac cycles				30 sec
[59]	0.88 MPa	1 kHz	20%		30 sec
[60]	0.8 or 0.6 MPa (PNP)	100 ms			12 min
[61]	$3\ \frac{W}{cm^2}$	100 Hz	20%		60 sec
[62]	$1\ \frac{W}{cm^2}$		10%		10 min
[63]	$2\ \frac{W}{cm^2}$		20%		30 sec
[65]	134 kPa (PNP)		20%		3 min
[66]	0.9 W	5 sec			10 min
[67]	$1.5\ \frac{W}{cm^2}$				2 min
[68]	$2\ \frac{W}{cm^2}$	20 sec	50%		6 min
[69]	$2\ \frac{W}{cm^2}$		50%		5 min
[70]		500 ms		1.6	20 min
[71]	1.8 MPa (PNP)			1.6	
[72]	$2.5\ \frac{W}{cm^2}$	2 Hz	50%		60 sec
[73]	$1\ \frac{W}{cm^2}$	10 Hz	50%		2 min
[75]	Four bursts of ultrasound delayed of 45 to 70 ms after R wave peak			1.4	
[76]				1.2 to 1.4	5 min
[77]				1.6	20 min

Reference	Target Organ or Model	Delivery Route	Frequency	Mode (CW/PW)	Pulse Duration
[78]	Four bursts 80 ms after peak of R wave			1.5	20 min
[79]	0.7 MPa; 1 MPa				
[80]	1 $\frac{W}{cm^2}$	2 Hz	50%		2 min
[81]	1 $\frac{W}{cm^2}$	2 Hz	50%		2 min
[82]	1 MPa and 1.2 MPa (PNP)			1.6	20 min
[83]	2.16 MPa (PNP)			1.6	4 min
[84]	5 $\frac{W}{cm^2}$ (optimal)				5 min
[85]				1.6	30 min
[86]	250 kPa (PNP)	3 kHz			5 min
[87]		1 kHz		0.4 to 0.45	20 min
[88]	1 MPa		50%		20 min
[89]	150, 300, 500 kPa (PNP)				
[90]	2 $\frac{W}{cm^2}$		20%		5 min
[91]				0.47	5 min
[92]	6 MPa (optimal)	100 Hz			1 min
[93]	0.21 MPa	970 kHz	20%		1 min
[94]				0.4 and 1.3	
[95]	1 $\frac{W}{cm^2}$				10 sec
[96]	2 $\frac{W}{cm^2}$		50%		160 sec
[97]				0.61	5 min
[98]	0.125, 0.25, 0.5, and 1 $\frac{W}{cm^2}$	10 Hz	50%		0, 5, 10, 15, 30, and 60 sec
[99]	1 $\frac{W}{cm^2}$	10 Hz	50%		2 min
[100]	3 $\frac{W}{cm^2}$		20%		60 or 120 sec

Reference	Target Organ or Model	Delivery Route	Frequency	Mode (CW/PW)	Pulse Duration
[101]	2.7 MPa (PNP)	13.9 Hz			90 sec
[102]	4 $\frac{W}{cm^2}$	10 Hz			2 min
[103]	0.5 $\frac{W}{cm^2}$		20%		10 sec
[104]	2 $\frac{W}{cm^2}$		50%		1 min
[105]	2 or 4 $\frac{W}{cm^2}$		25% or 50%		3 or 9 min
[106]	0.43 $\frac{W}{cm^2}$				10 min
[107]	3 $\frac{W}{cm^2}$		20%		1 min
[108]	0.27 MPa	21 ms	1%	0.2	31.5 min
[109]	0.4 $\frac{W}{cm^2}$	200 Hz	20%		5 min
[110]	0.4 $\frac{W}{cm^2}$	200 Hz	20%		
[111]	0.7 MPa (PNP)	100 Hz	50%		2 min
[112]				1	45 sec
[113]	0.02, 0.04, 1, and 2 $\frac{W}{cm^2}$				2.5 min
[114]	0.064 $\frac{W}{cm^2}$	0.5 Hz	50%		2 min
[115]	3 $\frac{W}{cm^2}$		20%		1 min
[116]	0.21 MPa			0.21	1 or 2 min
[117]	1 $\frac{W}{cm^2}$		20%		5 min
[118]	0.0182 and 0.026 MPa	100 ms			10 min
[119]	0.4 $\frac{W}{cm^2}$	200 Hz	20%		10 min

Reference	Target Organ or Model	Delivery Route	Frequency	Mode (CW/PW)	Pulse Duration
[120]	2 $\frac{W}{cm^2}$		50%		2 min
[121]	2 $\frac{W}{cm^2}$		50%		10 min
[122]	1 $\frac{W}{cm^2}$	2 Hz	50%		2 min
[123]	5 $\frac{W}{cm^2}$		50%		1 min
[124]	0.5 to 2 $\frac{W}{cm^2}$		50%		1 min
[125]	2 $\frac{W}{cm^2}$		50%		1 min
[126]	1 to 2 $\frac{W}{cm^2}$		10% to 50%		1 min
[127]				1	
[128]	2 $\frac{W}{cm^2}$		20%		5 min
[129]	2 $\frac{W}{cm^2}$		20%		5 min
[130]	2 $\frac{W}{cm^2}$		50%		10 min
[131]	0.5 $\frac{W}{cm^2}$				30 sec
[132]	2 $\frac{W}{cm^2}$		50%		5 or 10 min

As previously mentioned, sonoporation is the use of plasmid coated microbubbles paired with ultrasound. The microbubbles are transported throughout the various regions in the body

through blood vessels, and then are forced to undergo cavitation with ultrasound pulses which in turn results in the transfers of the plasmid constructs into the targeted organ and tissue cells.

Transfection is a process where DNA or RNA is delivered to cells [133]. The processes within the cell then take the DNA/RNA and use them to create proteins. These proteins then enable the cell to perform various functions. Transfection for the present work was used to regulate the glucose transfer across the placenta. The aim was to regulate glucose transport across the placenta to prevent fetal overgrowths. To accomplish this, the specific Glucose 1 Transporter (Glut1) was identified, and a specific plasmid construct was built to down-regulate the Glut1 gene.

The overall goal of this project was to develop successful strategies for preventing fetal overgrowth by manipulating the Glucose 1 transporter (Glut1) in the placenta *in vivo*. The work presented here shows the refining of sonoporation techniques to ensure a successful experiment.

The following are key ultrasound parameters that should be identified when performing sonoporation, which is graphically displayed in Figure 2.10:

1. Ultrasound Frequency (MHz)
2. Pulse duration (μs)
3. Pulse repetition period (ms)
4. Exposure time (s)
5. Duty Cycle, as a substitute for either the pulse duration or pulse repetition rate.

Additionally, when conducting sonoporation experiments there are many other factors that may affect the experiment of which key parameters are noted below:

1. Mouse breed
2. Plasmid characteristics
3. Microbubble characteristics (e.g. shell composition, average size)
4. Experiment protocol (e.g. injection of dox)
5. Microbubble delivery route.

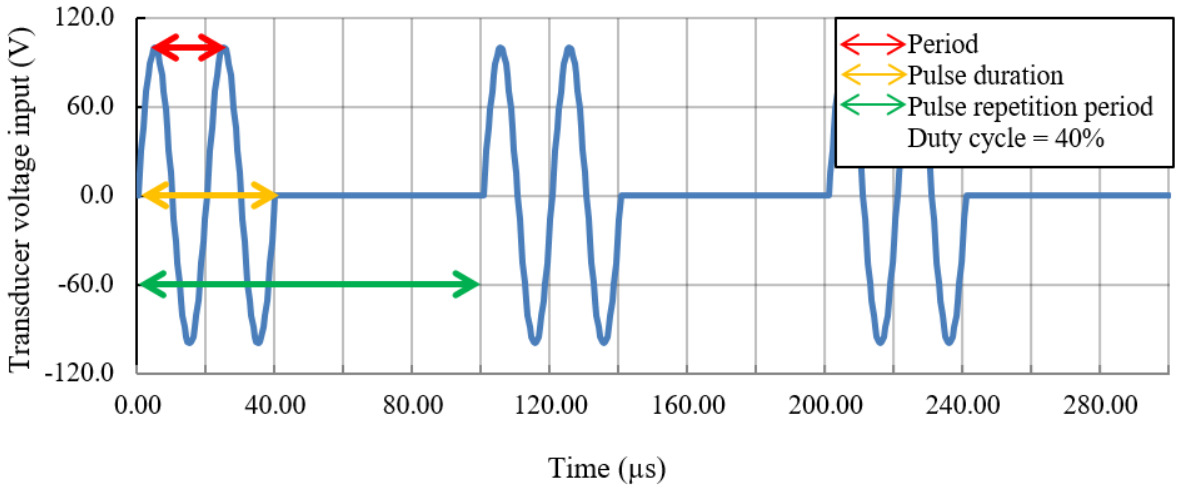

Figure 2.10: A visual representation of ultrasound parameters. The period is the inverse of the ultrasound frequency, and the exposure time is a summation of the total pulse repetition periods.

2.7 Sonoporation Design and Results

As previously mentioned, the sonoporation experiment process began with a DNA type that could be expressed in every tissue and organ. However, during the study the plasmid was switched to plasmids where the expression of the transgene is placenta-specific and inducible by doxycycline. The starting strategy when switching to any new DNA was to test whether expression within the liver was achievable. The liver was the first benchmark because we had previously established sonoporation experiments in mouse livers and both female and male mice could be

used for this experiment. Livers were also used because it is much easier to locate their position than a placenta.

There were three major plasmid types that were used throughout these experiments: pGL3, Genie3-GINbb-Ept1 (Ept1), and Genie3-GINbb-TRE3G-LUC-CYP-TRCN0000311403 (Glut1). Each plasmid served a different purpose. The pGL3 plasmid was used initially because we had established that microbubbles coated with it can be successfully delivered to a mouse liver. Additionally, it is not organ specific, meaning we can deliver pGL3 to any organ or tissue. Next the Ept1 plasmid was used because it is like pGL3 in the sense that it is not organ specific, however in order to induce the luciferase expression, an intraperitoneal (IP) injection of doxycycline must be added on the day of the sonoporation experiment. The Glut1 plasmid was used last because it was a placenta specific plasmid and we also needed to do an IP injection of doxycycline on the day of the sonoporation experiment. For both the Ept1 and Glut1 plasmid types we also tried to do IP injections of doxycycline the day before the sonoporation experiment to reduce the amount of doxycycline delivered per injection.

A typical sonoporation experiment involved the following steps:

Day one:

1. Preparation of microbubbles
2. Nair or shaving of mouse
3. Injection of microbubbles into mouse
4. Ultrasound treatment

Day two:

1. Intraperitoneal injection of luciferin into mouse
2. IVIS Imaging
3. Extraction if there is luciferase expression
4. Storage of data

In the case of using the Ept1 or Glut1 plasmid, there was an extra step prior to and on day one which involves the injection of doxycycline. The concentration of doxycycline was varied throughout testing as it was found higher levels often posed significant health risks to the mice. Fig. 2.11 shows the process flow for each plasmid type used in these experiments.

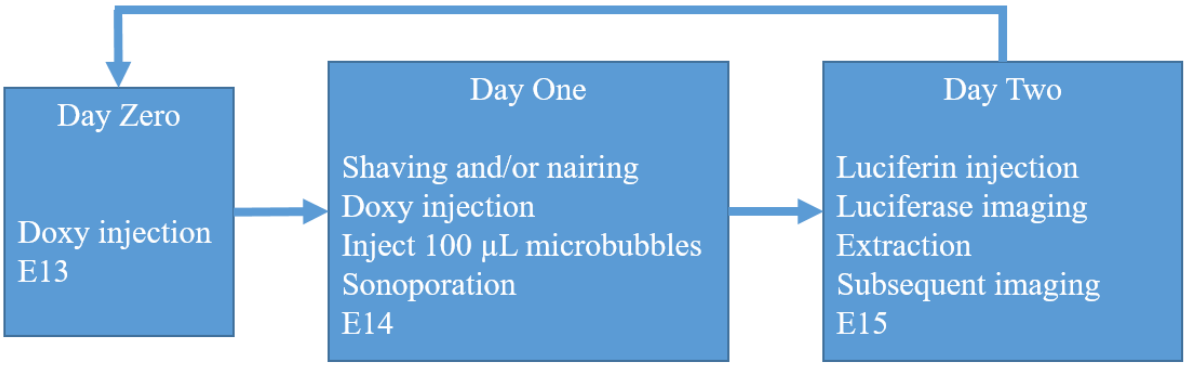

Figure 2.11: The typical sonoporation process. Ept1 and Glut1 needed doxy injections on day zero and one, however pGL3 did not need any doxy injection. In order to visualize the plasmids, 200 µL of luciferin needed to be injected into the mice intraperitoneally.

Initially microbubbles were infused via a tail vein injection. However, the poor efficiency of this technique became apparent, and was confirmed through comparative experimental trials. Therefore, it was determined that the best way to inject the microbubbles throughout the body was then to first inject the microbubbles into the cavity of the heart, specifically the left ventricle. The VisualSonics Vevo 2100 Imaging System was used to assist in imaging of the real time *in vivo*

injection of microbubbles. The transducer used in imaging operates with the same physics principles to the one that is used for cavitation, however the imaging transducer that was used in our experiments operates at frequencies that range from 32 MHz to 52 MHz, and is a phased array transducer, meaning there are many smaller transducers built into a single device. These individual transducers in summation provide a resolution and discernable image which can be interpreted by a sonographer. Fig. 2.12 shows the step by step imaging process of microbubbles being injected into the mouse heart.

The *in vivo* imaging system (IVIS), (Visualsonics Vevo 2100), is an imaging system which was purchased from Fujifilm, Toronto, ON, Canada. There are two main components to the IVIS, one being the software which controls the camera properties, and the other being the chamber where unconscious mice are placed to be imaged. The IVIS contains a camera and integrated system which has a sensitivity to light between 300 to 900 nm in wavelength. This allows for the imaging of visible light, and is also where the wavelength of firefly bioluminescence resides (at approximately 600 nm). The bioluminescence that the mice expressed due to luciferin injections was the same wavelength as the firefly. On the Living Image control panel (the software component of the IVIS system), properties such as the exposure time, binning, F/Stop, subject height, imaging mode, and field of view can be adjusted. These are summarized in Table 2.6.

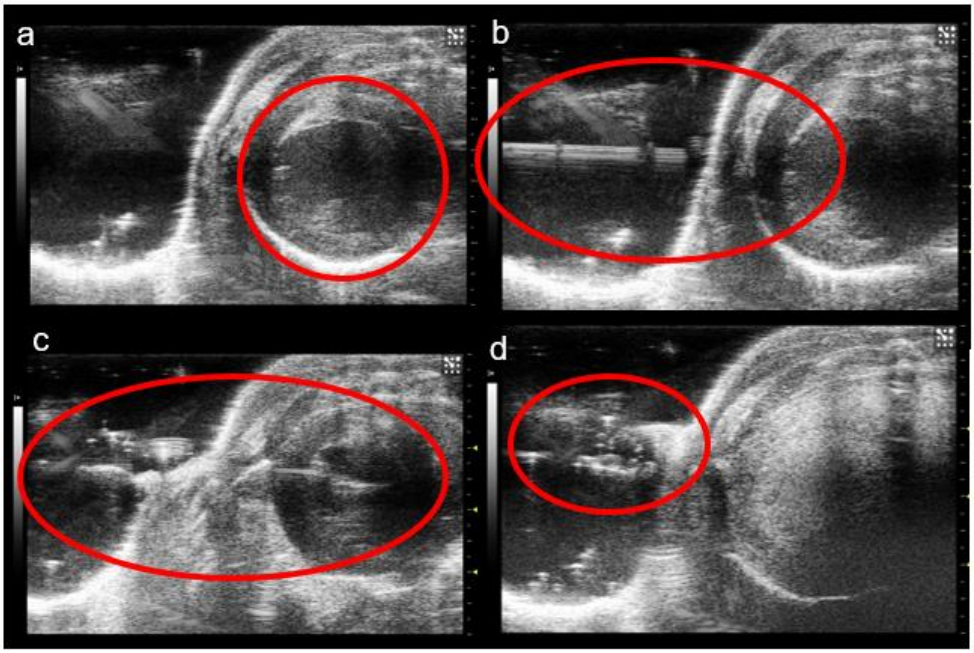

Figure 2.12: A microbubble injection procedure. In a the left atrium of the heart is circled, in b the 27 G needle is circled, in c the needle has just punctured the mouse heart and is ready to inject 100 µL of microbubbles, and in d the heart is shown with the microbubbles injected. Also, in d there are trailing air gaps in the ultrasound gel as well as some leakage of microbubbles which is circled.

Table 2.7: The Living Image control panel parameters and their definitions. By adjusting these parameters, the resulting display could be adjusted.

Parameter	**Definition**
Exposure Time	Duration that the IVIS measures photon activity from luminescence.
Binning	Grouping of luminescent pixels on an image, e.g. there are 4 medium binning groups in 1 large binning group.
F/Stop	Controls the shutter opening, the larger this value the more light allowed through.
Subject Height	Determines the stage height, or how near or far the objects are from the camera.
Imaging Mode	Luminescent and Fluorescent are the two different types of imaging methods available, a photograph option is also available but is best left as a checked box.
Field of View (FoV)	Adjusts image depending on how many subjects are being imaged. For example, an image with 5 mice requires a FoV of E but an image with one mouse or specific organs might only require an FoV of D or smaller.

2.8 RESULTS

The first trials of sonoporation focused on getting the pGL3 plasmid to work within the liver of SW mice. This task was accomplished in approximately 2 months, and Fig. 2.13 shows the results from some of these trials. Each SW mouse was injected with 200 µL of luciferin, and after 10 minutes were imaged for a duration of 2 minutes. Initially tail vein injections for the microbubbles were attempted, however these proved to be much too difficult and time consuming. Therefore, the heart injection method was performed for the microbubble injections. The concentration required for a single heart injection, a total yield of 800 µL of microbubbles per preparation, and the preparation of the mice for the experiments were constraints which lead the study to find four mice per experiment to be optimal. The goal of this process was to replicate previous results [YY], and once establishing gene transfection within the placenta incorporate the technique in placental gene delivery.

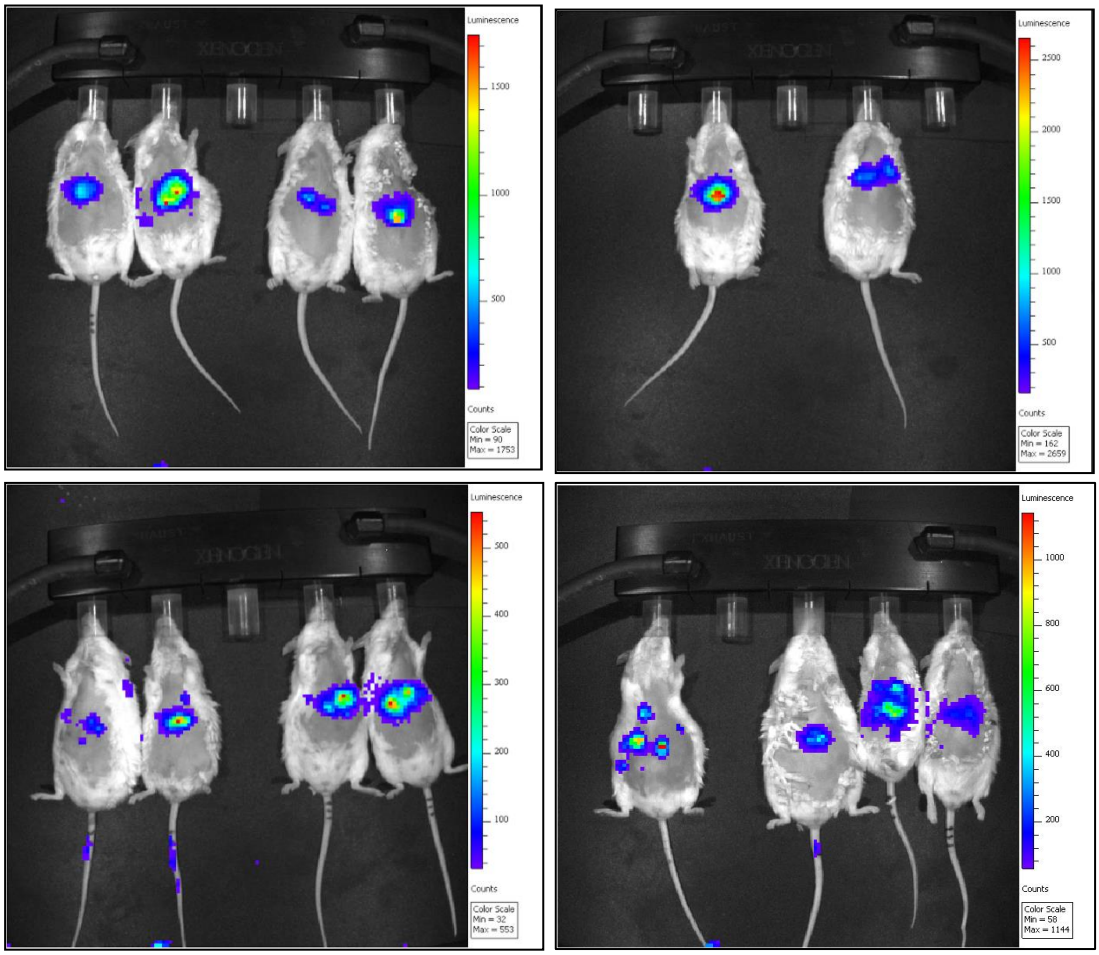

Figure 2.13: SW liver trials using the pGL3 plasmid images. Following these initial promising results from the SW trials, the C57BL/6 strain was used going forward.

Fig. 2.14 shows two mice which were used as controls and both injected with 200 µL of luciferin. In Fig. 2.14a the mouse had no microbubble injection and no sonoporation treatment, however in Fig 2.14b the mouse had a microbubble injection and an injection of luciferin. The luciferin concentration also impacted the experiments and a time lapsed image is shown in Fig. 2.15 and Fig. 2.16 for the C57BL/6 mice. Fig. 2.15 shows a concentration of 20 mg of luciferin substrate per 1 mL of PBS, and Fig. 2.16 shows a concentration of 50 mg of luciferin substrate per 1 mL of PBS. There was a two-minute exposure time for each image, and the first image for Fig. 2.15 and Fig. 2.16 began ten minutes after luciferin injection.

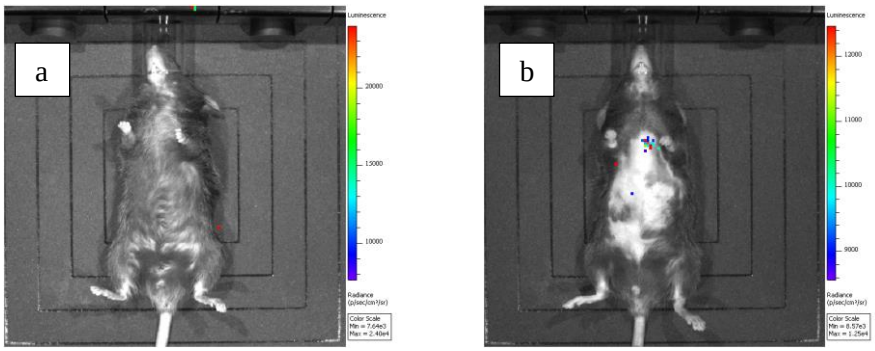

Figure 2.14: C57BL/6 control images with the pGL3 plasmid. Image (a) shows a mouse with no microbubble and luciferin injection as well as no sonoporation. Image (b) shows a mouse with microbubbles injected into the mouse, no sonoporation, and a 200 µL injection of luciferin.

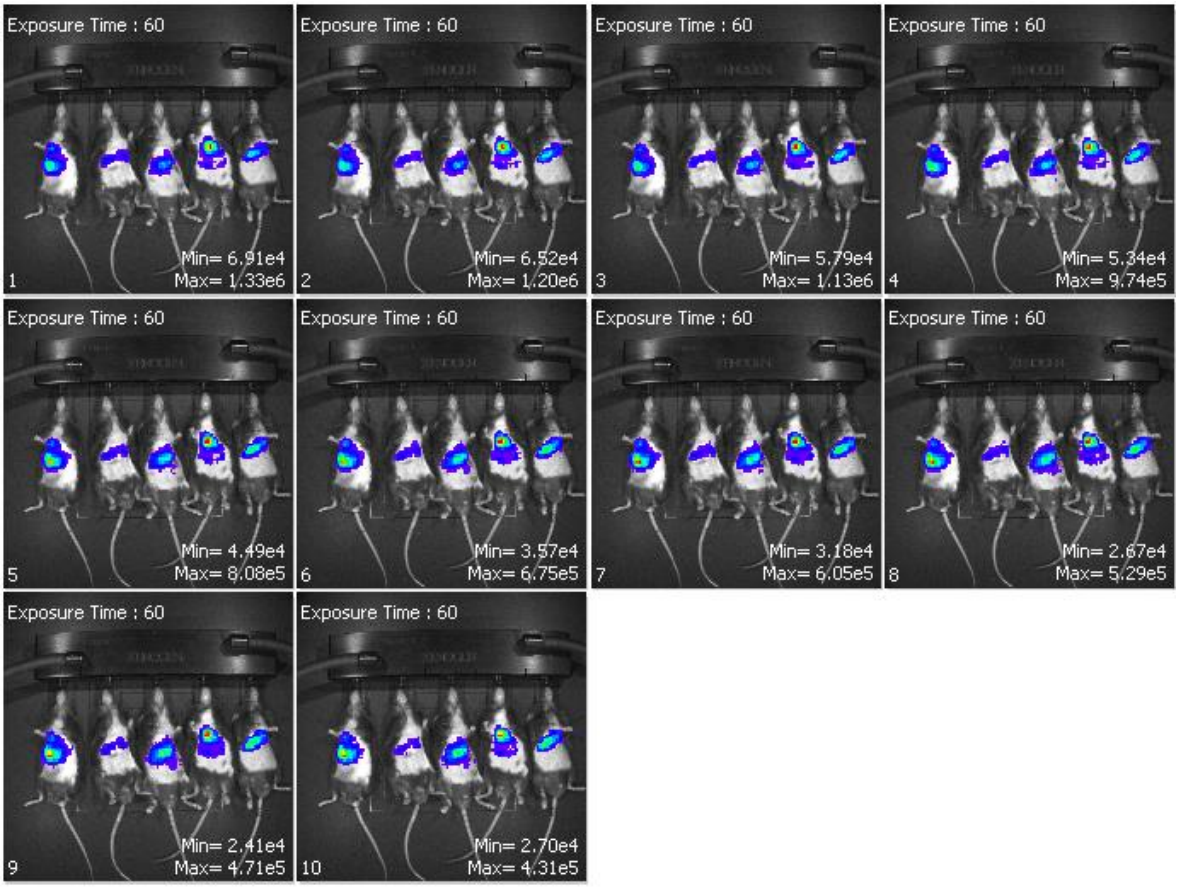

Figure 2.15: C57BL/6 liver trial pGL3 imaged with a luciferin concentration of 20 mg per mL. There is a three-minute separation time between each image. Peak expression was 1.33 M photons/sec/cm^2/sr and decreased to 0.431 M photons/sec/cm^2/sr by the tenth image.

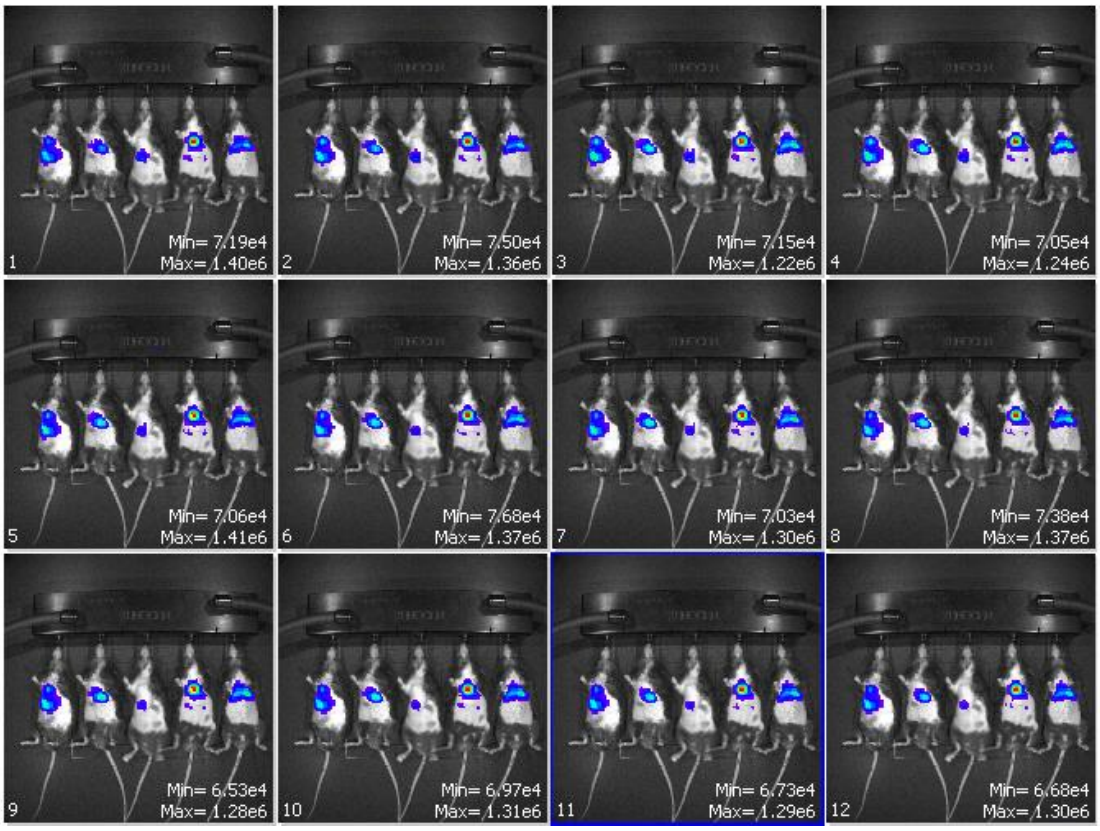

Figure 2.16: SW liver trial pGL3 imaged with a luciferin concentration of 50 mg per mL. This was found to be the optimal concentration of luciferin for IVIS imaging. Peak expression was 1.40 M photons/sec/cm^2/sr and decayed to 1.31 M photons/sec/cm^2/sr by the tenth image.

The next experiments were structured to deliver the pGL3 plasmid to the livers of the C57BL/6 mice. In addition to proving that similar ultrasound parameters can be used in both C57BL/6 and SW mice for liver trials, the pGL3 plasmid was also used as an ultrasound parameter check throughout the course of sonoporation experiments. The pGL3 plasmid assisted with verifying optimal ultrasound parameters, and throughout the course of this study was used as a check when the Ept1 and Glut1 plasmids were used. Some of the results from the pGL3 liver experiments are then shown in Fig. 2.17. The highest luciferase expression can be seen to be in the general area of the liver, or approximately where the liver should be. The IVIS initially takes a photograph of the unconscious mice prior to recording the photon count. After taking the photograph, the shutter is left open for a set exposure time while keeping track of the photons

leaving the target. This bioluminescent image is then overlaid on the original black and white photograph. Although making the quantification of luminescent activity much easier, this method does present some problems. Most notably, the results could be misinterpreted if a mouse moves during the imaging process, thus showing bioluminescent activity in incorrect places prior to overlaying the image. To ensure that mice moved as little as possible during the imaging capture process, mice were anesthetized three minutes prior to imaging, approximately seven minutes after the luciferin injection. Mice were also inspected prior to imaging to ensure proper anesthetization.

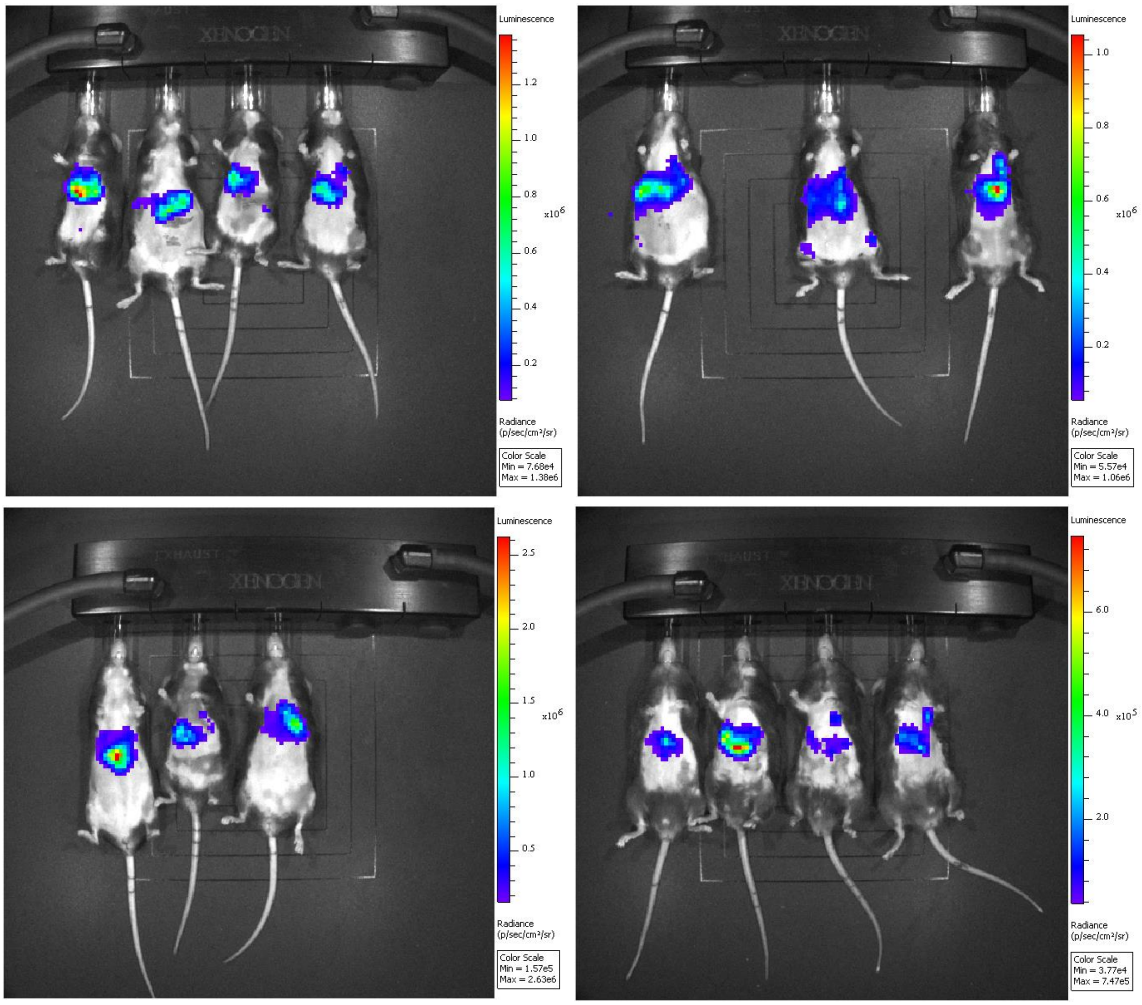

Figure 2.17: C57BL/6 pGL3 liver trial images. These images show that gene delivery to the liver using ultrasound was possible and repeatable. The light units are in photons/sec/cm^2/sr. The bioluminescence was found to be largest in the liver for many of these experiments.

Although Fig. 2.17 showed that liver gene delivery was possible, it did not validate that the gene delivery was taking place in the liver. To verify that ultrasound targeted gene delivery to the liver the mice were sacrificed and their livers were extracted for subsequent imaging. Some of the extracted livers using the pGL3 plasmid are shown in Fig. 2.18, validating that the largest luciferase expression was in the liver.

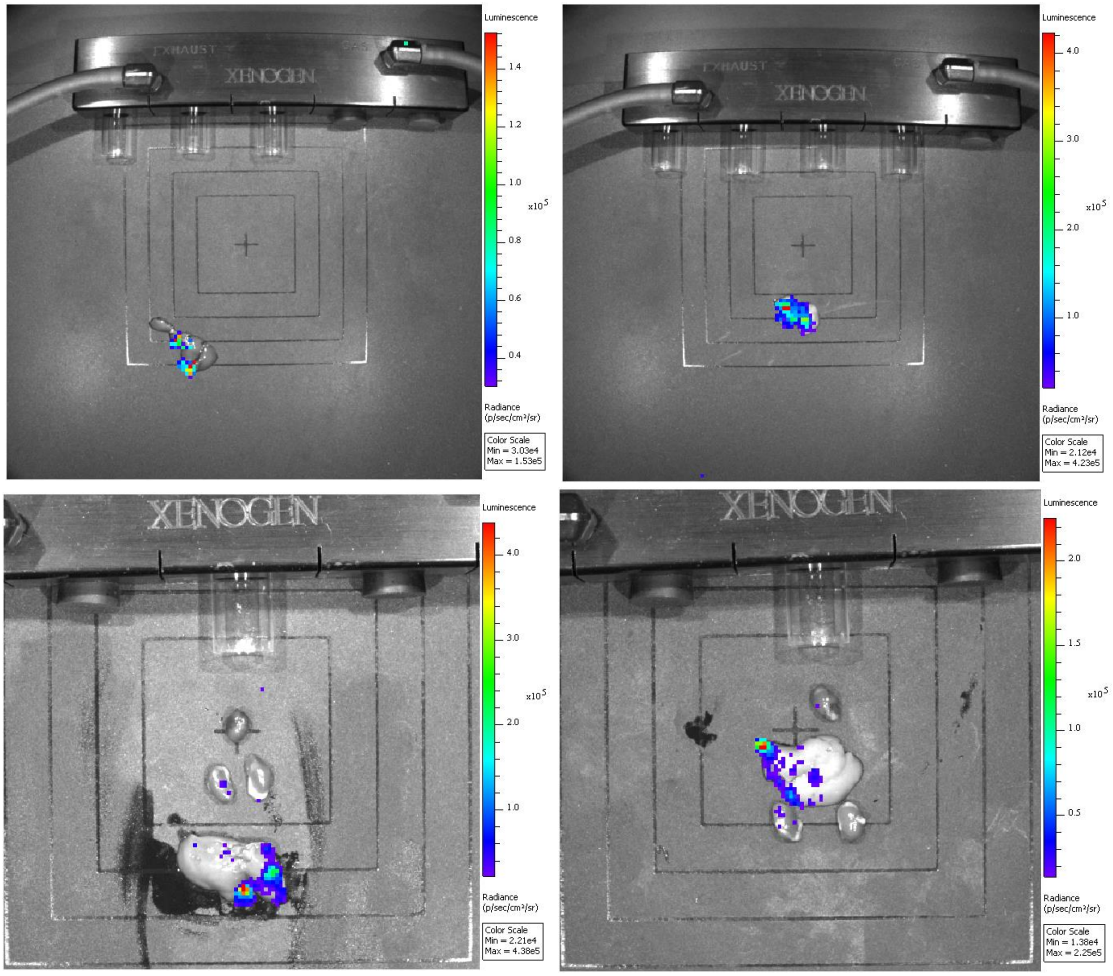

Figure 2.18: Extraction of livers from the pGL3 experiments. For successful experiments, the liver was either the highest expression of bioluminescence or was the only organ which showed luciferase expression.

After achieving successful gene transfection into the livers, gene transfection into the placentas of pregnant C57BL/6 mice were performed. Fig. 2.19 shows some of the C57BL/6 mice which were used in placental tests with the pGL3 plasmid. Fig. 2.19 shows only one mouse in

three separate images and a group of mice in the final image. Experiments of four mice were followed up with individual photographs the next day, and were taken to adjust for the luciferin expression in each mouse. The initial hypothesis was that the imaging software could only display the luciferin concentration from the mouse yielding the largest luciferin activity. However, through repeated images it was found that the number of mice in an image does not impact the radiance count for each mouse, only the visual intensity compared with the scale bar is impacted.

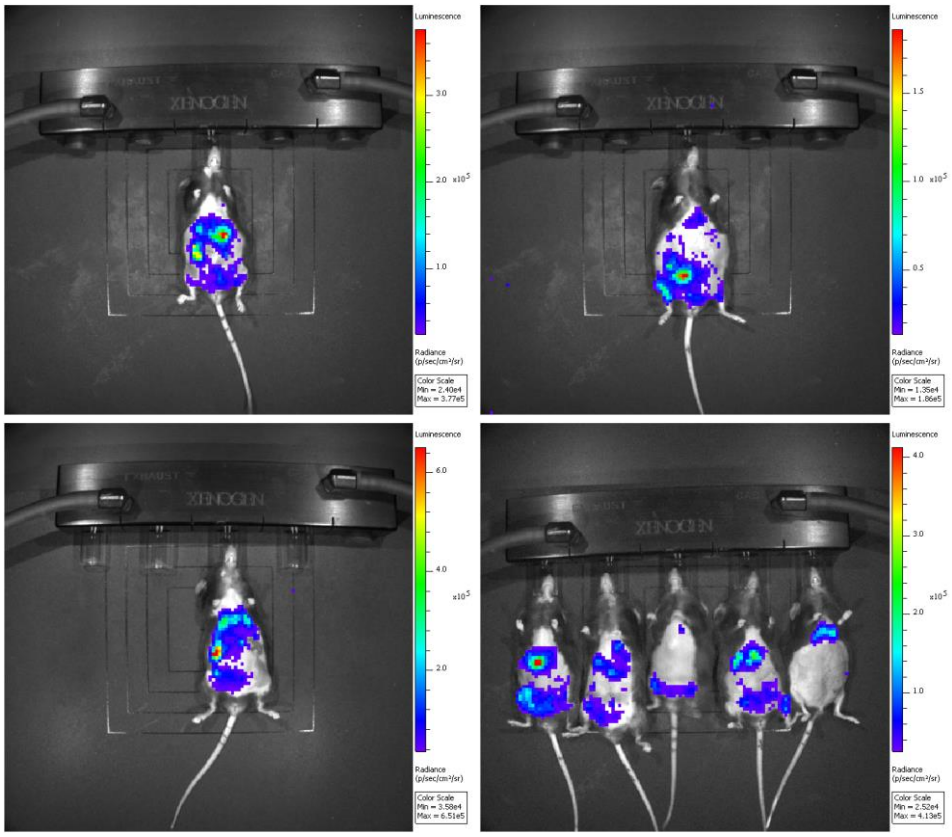

Figure 2.19: Placental trials with the C57BL/6 mouse using the pGL3 plasmid. Experiments using the transducer to target specific placentas were not successful, however gene transfection to the placenta was established.

The uterine horn of the mouse was first extracted to verify that there was luciferase expression in that region of the mouse as shown in Fig. 2.20, and then subsequent images of placentas were taken as shown in Fig. 2.22. A mouse image was first taken to visualize if there was any luciferase expression within the placental region of the pregnant mouse. The uterine horn

was then quickly extracted and imaged to provide clues to whether there was bioluminescence coming from either the fetuses or placentas, and followed up with images of the fetuses and placentas both together and separated.

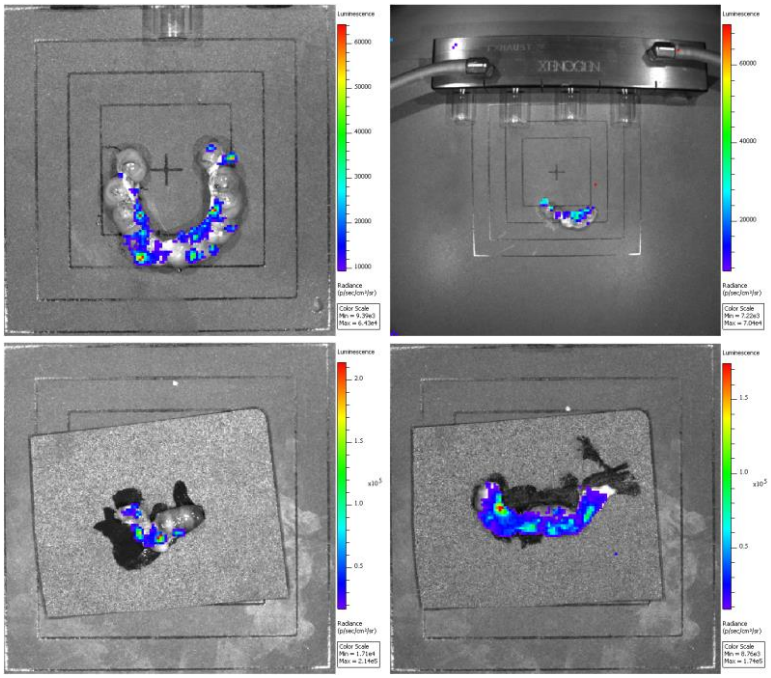

Figure 2.20: Images of the uterine horn using the pGL3 plasmid. If luciferase activity was recorded in these images, further extraction of both fetuses and placentas were performed.

Following the success of the pGL3 plasmid in the B6 mouse placentas, Ept1 plasmids were used. As a reminder, this plasmid will only express luciferase when there is an IP injection of doxycycline on the day of the sonoporation experiment. The concentration of doxycycline in the IP injection was varied between 1 mg/kg, 25 mg/kg, 50 mg/kg, 100 mg/kg, and 200 mg/kg each with a total injection volume of 300 µL. These concentrations amounted to a total of 0.025 mg, 0.625 mg, 1.25 mg, 2.5 mg, and 5 mg injected doxycycline for each respective concentration. Both Ept1 and Glut1 have not yet been successful due to complications with identifying an optimal concentration of doxycycline, however work is still being done to do so and some preliminary results are shown in Fig. 2.22 for the Ept1 plasmid in use with liver gene transfection.

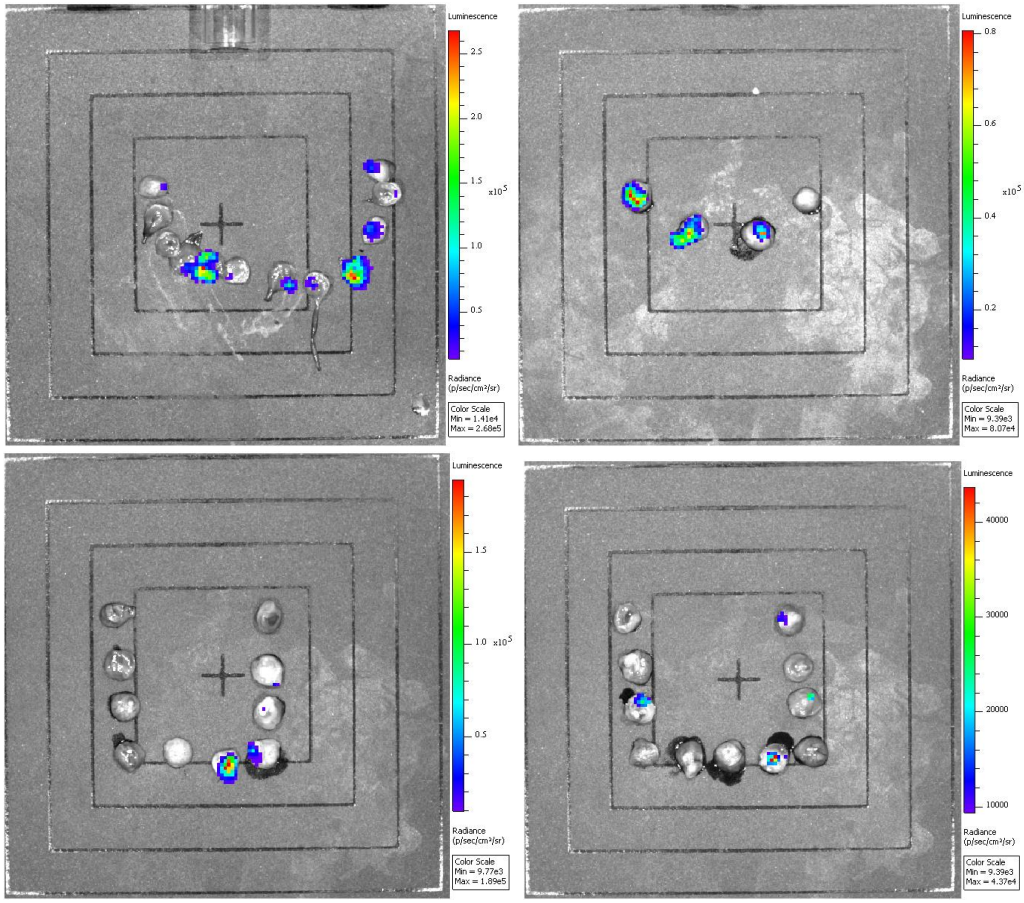

Figure 2.21: Images of the C57BL/6 mouse placentas using the pGL3 plasmid. These images show that placental gene delivery with the pGL3 plasmid is possible.

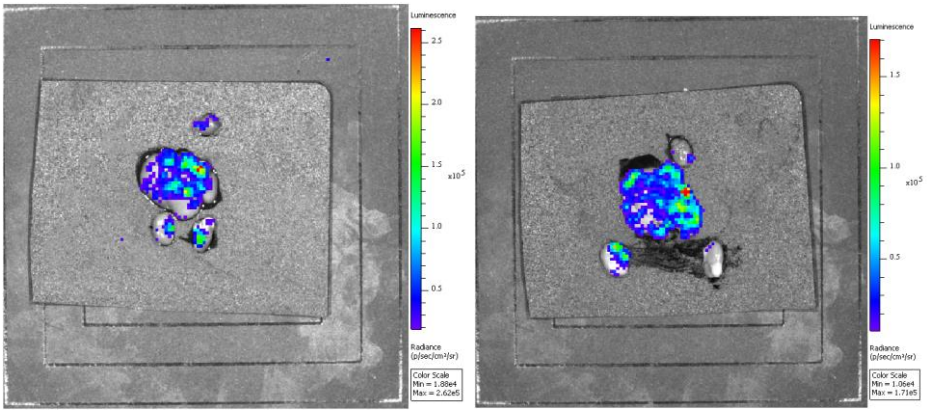

Figure 2.22: Preliminary testing using the Ept1 plasmid for liver trials. The concentration of doxycycline was 20 mg/kg in these experiments, however the mice looked in poor health. Experiments are currently underway to reduce the concentration of doxycycline but still ensure a successful experiment.

2.9 DISCUSSION

One of the most important factors determining the success of a sonoporation experiment was the quality of heart injection. A poor heart injection not only puts the mouse at risk but also increases the decreases the likelihood that the microbubbles are properly delivered to the correct organ. This was one of the motivating factors for introducing the grading scheme about midway through this project. We determined that heart injections of microbubbles are superior to tail vein injections not only in terms of the injection difficulty but also in microbubble delivery efficiency. Heart injections which scored above a 2 would yield higher success rates than injections scored less than 2, however an injection which was scored less than 2 would result in a failed experiment or even worse, death of the mouse. Some selected results for both the liver and placental trials using the pGL3 plasmid are shown in Table 2.8.

Table 2.8: Selected results from sonoporation experiments. These experiments used the pGL3 plasmid and targeted either the placenta or liver.

Key	
Score - quality of heart injection	From 0 to 3, 0 being a poor injection and 3 being an optimal injection of microbubbles
Luciferase expression – did the mouse express bioluminescence	No = N Yes = Y
Mouse breed	Swiss Webster = SW C57BL/6 = C
Target organ	Liver = L Placenta = P
Transducer	GE unfocused = GE Olympus focused = O

Date	**Input Voltage (mVpp)**	**Pressure (MPa)**	**Score (0 to 3)**	**Luciferase expression**	**Mouse Breed**	**Target Organ**	**Transducer**
4/4/16	650	1.55	3	Y	0	L	GE

			3	Y		L	
			3	Y		L	
			3	Y		L	
8/3/16	650	1.55	3	Y	1	P	GE
			1	Y		L	
			3	N		L	
			3	Y		L	
			3	Y		L	
			2	N		L	
9/5/16	650	1.55	3	Y	1	L	GE
			0	N		L	
			3	Y		L	
			3	Y		L	

12/19/16	250	3.42	3	Y	1	L	O
			2	Y		L	
			3	N		L	
			3	N		L	
			3	N		L	
12/24/16	350	3.5	2	Y	1	P	O
			2	N		P	
			2	N		L	
			3	Y		L	
			2	Y		L	
12/26/16	250	3.42	3	Y	1	L	O
			3	Y		L	
			3	Y		L	

			3	Y		L	
			3	Y		L	
1/10/17	2.5	3.42	1	Y	1	L	O
			1	N		P	
			1	N		L	
			1	Y		L	
			1	Y		L	
1/25/17	250	3.42	3	Y	1	L	O
			3	Y		L	
			3	Y		L	
1/26/17	250	3.42	3	Y	1	L	O
			3	Y		L	
			3	Y		L	

			3	Y		L	
1/27/17	250	3.42	3	Y	1	L	O
			3	Y		L	
			3	Y		L	
			3	Y		L	
2/1/17	250	3.42	3	Y	1	L	O
			3	Y		L	
2/6/17			3	Y		L	GE
			3	Y		L	
			3	N		L	
			3	Y		L	
2/7/17			3	N		P	GE
			3	Y		L	

			3	Y		P	
			3	Y		P	
2/8/17	700	3	3	Y	1	L	GE
			3	Y		L	
			3	Y		L	
			3	Y		L	
			3	Y		L	
2/9/17	700	3	3	Y	1	L	GE
			3	Y		L	
			3	Y		L	
			3	Y		L	
2/12/17			3	N		P	GE
			3	Y		P	

			3	Y		P	
			1	N		P	
2/13/17			3	N		P	GE
			3	Y		P	
			3	Y		P	
			3	Y		L	
2/14/17	700	3	3	Y	1	L	GE
			3	N		P	
			3	Y		L	
			3	Y		L	
2/15/17	700	3	3	Y	1	L	GE
			3	N		P	
			3	Y		L	

			3	Y		L	
2/17/17	700	3	2	Y	1	L	GE
			2	Y		L	
			2	Y		L	
			0	N		L	
2/19/17	700	3	3	N	1	P	GE
			3	N		P	
			3	Y		L	
2/21/17	700	3	2	N	1	P	GE
			2	Y		L	
			3	Y		L	
			2	Y		L	
2/22/17	700	3	3	Y	1	L	GE

			3	Y		L	
			3	Y		P	
			3	Y		L	
2/23/17	700	3	3	Y	1	L	GE
			2.5	N		P	
			3	Y		L	
			3	Y		L	
2/27/17	700	3	2	N	1	P	GE
			3	Y		P	
3/15/17	700	3	3	N	1	P	GE
			3	N		P	
			3	Y		P	
			3	Y		P	

3/16/17	700	3	2	Y	1	P	GE
			2	Y		P	
			3	Y		P	
			3	Y		P	
			3	N		P	
3/22/17	700	3	2	Y	1	P	GE
			3	Y		P	
5/3/17	700	3	2.5	Y	1	P	GE
5/8/17	700	3	2.7	Y	1	P	GE
5/15/17	700	3	1	N	1	P	GE
			2	Y		P	
			2	N		P	
5/17/17	700	3	2.9	Y	1	P	GE

			2.9	Y		P	
6/28/17	700	3	2.4	Y	1	L	GE
			2.4	Y		L	
			2.4	Y		L	

Throughout the course of these experiments the exposure time for sonoporation was best below 5 minutes to ensure that there would be no negative effects from either heating or shear stress from the transducer. The other ultrasound parameters which were found to be optimal was an input voltage of 700 mV, a 15 ms pulse duration, a 375 ms pulse repetition period, and a one-minute exposure time. The luciferin concentration (delivered via IP injection) used in IP injections was also determined to be optimal at a concentration of 75 mg per mL in a total volume of 200 µL. The lowest luciferin concentration that was found to be feasible for use in imaging was 30 mg per mL, and the only difference between this and the optimal luciferin concentration was the duration at which the luciferase expression persisted. As illustrated in Table 2.7, for the liver experiments a 88.67% success rate was achieved, and for placental trials a 57.89% success rate was achieved using the pGL3 plasmid.

CHAPTER 3 IMPEDANCE SPECTROSCOPY FOR THE QUANTIFICATION OF ARTEMIA CYST DEVELOPMENT

Embryos are formed when an oocyte (egg) has been fertilized with sperm. The process of fertilizing oocytes out of the body and in a controlled lab environment is called *in vitro* fertilization (IVF). Currently, a technique known as intracytoplasmic sperm injection (ICSI) is used to insert a single sperm into an oocyte to create an embryo [134]. The embryos are then subjected to a morphological grading process which separates the low-quality and high-quality embryos. The higher-grade, high-quality embryos are then implanted in the womb, which ideally leads to pregnancy.

There are two major industries which use IVF, namely human and bovine IVF. In both industries, the morphological grading procedure is used for embryos. For human embryos, a biopsy is also performed in addition to the morphological grading [135]. Human embryos are slightly punctured when they are in the two- to four-cell stages, and when they reach the blastocyst stage the cells permeate out of the shell. Approximately two cells are extracted from the blastocyst, and cut from the other cells with a laser. The biopsy provides crucial information such as the genetic abnormalities (aneuploidy) that may exist within the blastocyst. Although it is a crucial step in IVF, this procedure is highly invasive to the developing embryo. Therefore, a non-invasive viability test for these embryos is necessary.

In the human IVF market, the Embryoscope takes images every five minutes during embryo incubation [135]. The clinician and patient can then look over these incremental photos to interrogate the development of these embryos. The Embryoscope also provides detailed files which contain matrices of information about the embryo's growth. However, the Embryoscope fails to

provide an alternative to the golden standard of biopsies because IVF doctors are still relying on the biopsy, and often provides the clinician and patient with too much data on the embryo's growth, leading to some confusion [135].

Impedance spectroscopy (IS) is a possible alternative to biopsies which could also possibly be integrated within the Embryoscope. This technique measures the impedance of an embryo over a range of frequencies. In this chapter, the correlation of developmental changes of *Artemia* cysts to impedance changes are discussed [136].

3.1 Cells used in Impedance Spectroscopy

There have been some studies with IS with cells [137, 138, 139, 140]. [137], [138], and [139] used IS as a tool for differentiation between cells, and employed the use of a differential cell impedance measurement. [140] is a review paper which showed the various methods of using IS to investigate different various characteristics about cells such as the opacity (the ratio between a high-frequency impedance and lower-frequency impedance), membrane capacitance, and cytoplasm conductivity. In these publications, the cells which were studied included red blood cells, white blood cells, erythrocytes, lymphocytes, and monocytes, among others. We investigated embryos of the *Artemia* brine shrimp. This study aimed to build on these works by investigating the possible correlations between IS and the embryological developments of the *Artemia*.

3.2 Experimental Design

The animal model that was used for the IS experiments was the *Artemia*. This model was chosen because of the low cost and ease of accessing the cysts.

The *Artemia* is a type of brine shrimp which undergo a process known as diapause. In extreme environmental conditions, such as extreme heat or cold, the diapause cycle of the *Artemia* cysts protect them from dying by reducing metabolic activity to a near zero value. These cysts are often subjected to dehydration when the pools of water that they live in go dry, however if water returns to these pools then the cysts go through a rehydration process which eventually leads to their hatching. We acquired our cysts through a local grocery store, and could successfully carry out experiments with them.

3.3 MODEL

The equivalent circuit model for a cell is shown in Fig. 3.1. This equivalent circuit includes a double layer capacitance on each electrode, impedances and capacitances for the cell and interior of the cyst, and the capacitance and impedance of the liquid media. This model of the experimental environment provides insight into the impedance as a function of frequency for the cyst and the surrounding liquid media.

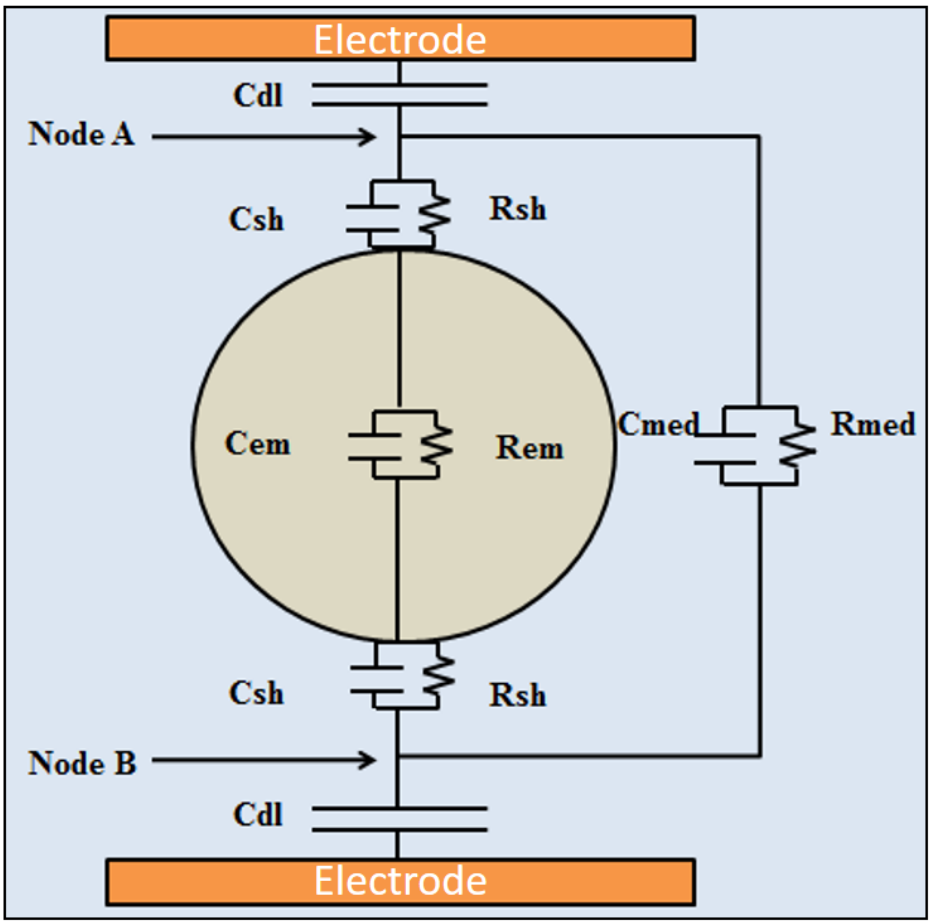

Figure 3.1: Equivalent circuit model for a cell, adapted from [136]. This circuit is a simplification of the cell and models the impedance contributions from the shell, inner embryo, and surrounding media.

The circuit elements shown in Fig. 3.1 are characterized by Equations (3.1) to (3.6) below [141, 142, 143]. In these equations, Cdl, Csh and Rsh, Cem and Rem, and Cmed and Rmed are the capacitances and resistances of the electrical double-layer, shell, embryo, and media, respectively.

$$Z_t = 2 * Z_{dl} + [(Z_{sh} + Z_{em})]||Z_{med}]$$

$$= 2 * Z_{dl} + \frac{2*Z_{sh}*Z_{sol}*Z_{em}*Z_{med}}{2*Z_{sh}+Z_{em}+Z_{med}} \quad \text{(Eq. 3.1)}$$

$$Z_{sh} = Z_{Rsh}||Z_{Csh} = \frac{R_{sh}}{j*\omega*R_{sh}*C_{sh}+1} \quad \text{(Eq. 3.2)}$$

$$Z_{em} = Z_{Rem}||Z_{Cem} = \frac{R_{em}}{j*\omega*R_{em}*C_{em}+1} \quad \text{(Eq. 3.3)}$$

$$Z_{med} = Z_{Rmed}||Z_{Cmed} = \frac{R_{med}}{j*\omega*R_{med}*C_{med}+1} \quad \text{(Eq. 3.4)}$$

$$Z_{dl} = \frac{1}{j*\omega*C_{dl}+1} \quad \text{(Eq. 3.5)}$$

$$C_{dl} = \frac{\varepsilon*A}{d} = \frac{\varepsilon*A}{L_d} \quad \text{(Eq. 3.6)}$$

The double layer capacitance, C_{dl}, at the electrode contacts depends on the Debye length, as shown in Equation 3.6. The Debye length can be solved for using

$$L_d = \sqrt{\frac{\varepsilon*\kappa_B*T}{2*Z^2*q_e^2*C_0}} \quad \text{(Eq. 3.7)}$$

where ε is the permittivity, k_B is Boltzmann's constant, T is the absolute temperature, z is the count of valence ions in the solution, q_e is the elementary charge value, and C_0 is the molar concentration of ions.

The *Artemia* cysts were smaller than the electrodes used in the study, making the impedance contribution from the media an important factor consider. The 100 μm radius cyst was placed between two 250 μm radii conductors, and can be replaced by a circuit equivalent Z_{cyst} between nodes A and B. Z_{med} is then the modeled impedance contribution from the surrounding media, which in this case was salinized natural spring water. Z_{med} is in parallel to Z_{cyst}, and has a significant contribution to the overall impedance changes of the circuit. Another contribution to the overall impedance stems from the electric double layer, Z_{dl}. This term cannot be negated since the media used had a significant ionic concentration of salts. Therefore, the circuit modeled in Fig. 3.1 provides an understanding of each circuit element and their underlying contribution to the overall impedance as measured using the electrodes. Two separate measurements were then taken in the experiments, one with the cyst between the electrodes and one with only the aqueous media between the electrodes. The differential impedance was then calculated by subtracting the media-only measurement from the cyst measurement. Fig. 3.2 shows the measured change of impedance as the frequency of a 1 V_{pp} ac signal was swept from 1 kHz to 1 MHz. The impedance changes as a function of frequency as different impedances dominate (from the cyst or the surrounding media). A frequency of 1 kHz was selected for impedance measurements over the cyst development period, as it has a high magnitude, and the impedance values near that frequency vary linearly over a smaller range than at the higher measured frequencies.

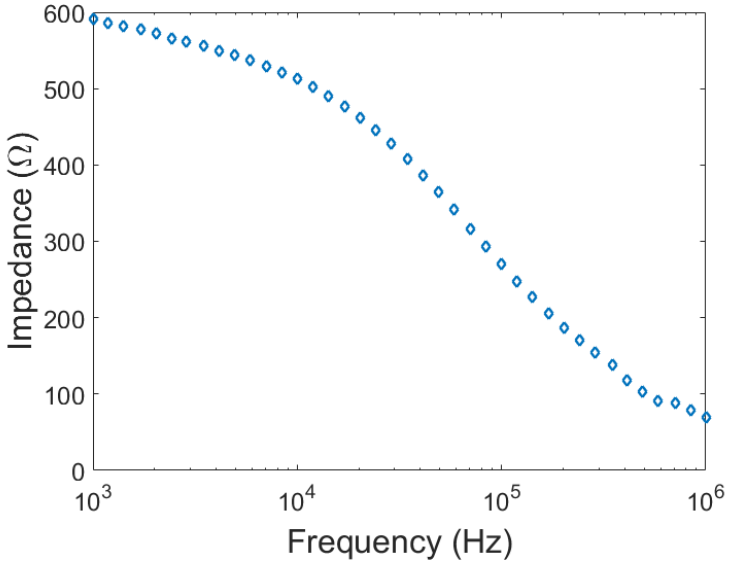

Figure 3.2: Experimentally measured data from a single cyst measured during the pre-emergence development phase. Experimentally measured data from a single cyst measured during the pre-emergence development phase. A frequency of 1 kHz was selected for the measurement of impedance over the embryo development period, as it has a high impedance magnitude, and the impedance has a relatively small linear variance about this frequency.

3.4 Design and Fabrication

Rapid prototyping is a procedure involving a quick fabrication of a model of a final product. This model provides insight into the various properties of the final product, such as the material type, durability, and strength. We employed this methodology into our construction of microfluidic channels for the *Artemia* experiments.

Polydimethylsiloxane (PDMS) is a type of elastomer which was used to construct the microfluidic channels used here. The elastomer comes in two parts, a base and a curing agent. To make the PDMS, 10 parts of the base agent was mixed with one part of the curing agent (weight ratio) for approximately 15 minutes to 30 minutes depending on the consistency of the mixture. The combined mixture was then placed into a vacuum chamber to remove any gas impurities in

the mixture for one hour. Depending on the type of channel that was built, the PDMS was then either poured into a mold or added as a sealant between the glass slides as well as channel cover. This step ensured that the channel remained airtight. The PDMS was then placed into an oven at 80 ˚C to cure. To bond PDMS to glass or other PDMS constructs, a corona treatment was employed [144] and a light pressure applied to the two sides of materials until they were completely bonded.

Initially, a PDMS mold was used for the *Artemia* channel, however this was later abandoned for several reasons. Making a full PDMS channel took a significant amount of time compared to a rapidly prototyped channel, and the secondly there were constant leaks in the PDMS channel compared to the rapidly prototyped channel.

The rapidly prototyped channel had a bottom layer consisting of a 1-mm-thick glass substrate. Four 38.1 mm x 25.4 mm x 1 mm-thick glass microscope slides were bonded to the glass substrate using clear double-sided tape, and a 500-µm-diameter copper wire was embedded between each pair of glass slides along the x-direction, as illustrated in Fig. 3.3. The channel dimensions were built to accommodate the *Artemia* cysts which range from 200 µm to 230 µm in diameter.

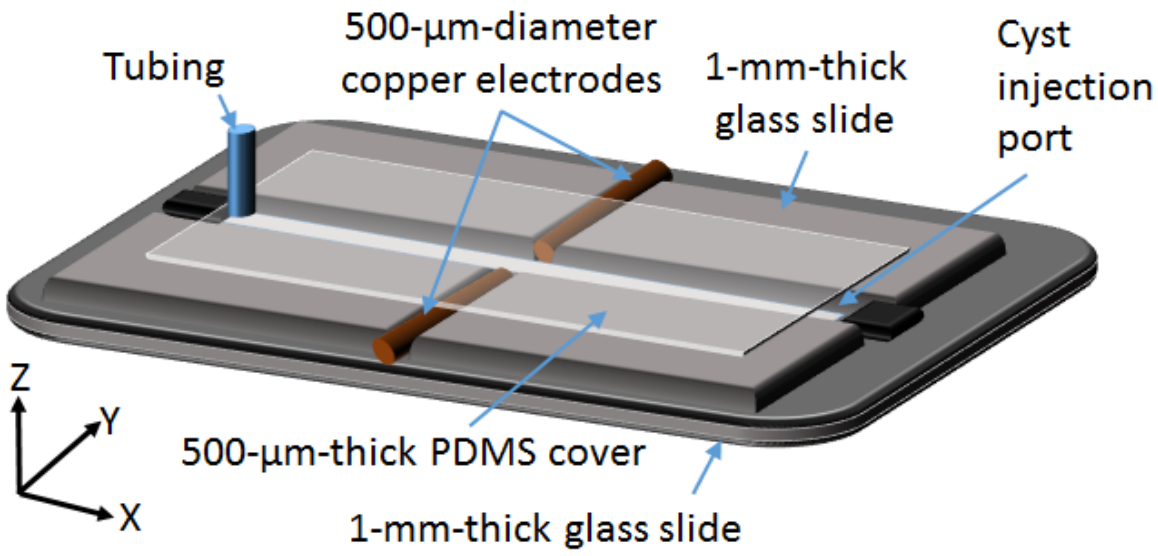

Figure 3.3: The microfluidic device used for measuring impedance changes in brine shrimp cysts, adapted from [136]. The channel was fabricated taping four 38.1 mm x 25.4 mm x 1 mm glass slides on top of a glass substrate. Two copper electrodes were embedded along the channel. The channel ceiling is made of 500-µm-thick PDMS. The channel floor was coated with PDMS to create a channel depth of 600 µm. The brine shrimp cyst was injected through the opening at one end of the channel.

3.5 Experimental Setup

The *Artemia* cysts undergo a process called dormancy when they encounter extreme environmental conditions such as dehydration. Dormancy can be further looked at as two separate events: diapause and quiescence. During diapause, the cyst resists hatching by stunting biological growth, even under favorable circumstances [141, 145]. Quiescence occurs when the cyst is exposed to extreme environmental conditions terminating diapause, and forcing the cyst to enter a hypometabolic state [141, 145]. In this state, the cyst can survive for months to several years [141, 145, 146, 147]. The measurements in this work took place between the period of quiescence and the eventual hatching of the *Artemia* larva.

All *Artemia* cysts in this study were purchased in the quiescent stage. Under favorable conditions, a healthy cyst can rehydrate and hatch within 24 hours [148, 149]. After acquiring the cysts, they were placed in a 100-mm-diameter petri dish with a salt mixture. Store-bought natural spring water was then mixed with the salt and the cysts, and 20 cysts were visually inspected and separated into individual petri dishes using handheld tweezers. Floating cysts, empty cysts, and cysts with irregular morphology were not used in this experiment. The experiments were carried out at approximately 25 ˚C, and the cysts were illuminated by an incandescent desk lamp. The combination of the temperature and illumination created a favorable hatching environment for the cysts.

After carefully placing a single cyst at the cyst injection port using stainless-steel tweezers, the cyst was then positioned between the electrodes with a syringe pump. The impedance was then measured using an impedance analyzer (Hioki IM 3570). The positioning of the brine shrimp cyst was observed with a CMOS camera (Point Grey Flea3-U3-20E4C) mounted on a camera lens (Nikon Micro Nikkor 60 mm). The *Artemia* cysts were suspended in salt water at a pH of approximately 7.6.

The magnitude and phase were measured with a 1 V_{pp} ac signal sweeping from 1 kHz to 1 MHz at 400 discrete frequencies. The impedance measurements were conducted at varying time intervals over a period of 24 hours, or until hatching of the brine shrimp was visually observed. The reported impedance and phase data were calculated by taking the difference of an impedance measurement with the cyst between the electrodes and an impedance measurement with no cyst (only the salinized water). The first measurements were taken when the cyst looked like the image in Fig. 3.4A, and the last measurements were taken when the cyst looked like the image in Fig. 3.4C. Fig. 3.4A shows a dehydrated cyst, and it what the cyst initially looked like. Fig. 3.4B shows

a fully hydrated cyst which would typically be seen at 12 hours into the experiment. Fig. 3.4C and 3.4D then show the *Artemia* larva emerging and eventually hatching from the cyst, respectfully. A total of 20 cysts were measured in this experiment.

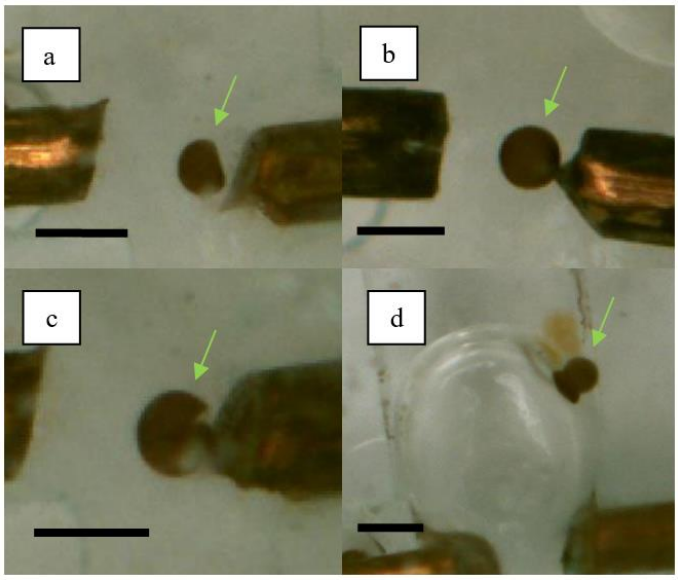

Figure 3.4: Artemia cyst development during this study, adapted from [136]. Most of the cysts began with a shape like the one shown in (a). These cysts are deformed due to the dehydration of the cyst. The engorged cyst shown in (b) is typical as the cyst approaches complete hydration. A cyst hatching is shown in (c), and an almost completely hatched Artemia is shown in (d). All scale bars are 500 μm. The green arrow in each image points to the Artemia cyst. 20 total cysts underwent interrogation during this experiment. Air bubbles, as illustrated in (d), did not significantly affect measurements however they were difficult to remove once they were introduced into the microfluidic channels. Some ways that they got into the channels were either through leaks within the electrode channels themselves, accidental injection through the syringe, or from the poor sealing of the microfluidic channel (e.g. electrode channels or poor sealant for tubing connected to syringe pump). Fortunately, the channels presented in this paper are relatively simple and can be quickly reproduced in under four hours. Additionally, several channels can be fabricated for a maximum of five microfluidic channel every four hours.

3.6 RESULTS

The Artemia cysts are hypometabolic if their hydration levels are below 10% and can be stored for long periods of time without losing viability [150]. In the presence of water, the cysts begin to hydrate, and if favorable conditions are present, hatch. The metabolic processes with the

cyst start if the hydration level is over 10%. Metabolism increases significantly as the hydration level increases, and hydration can reach 140% of the initial level within an hour [150].

There are three developmental phases of the *Artemia* cysts, and they occur after reaching the 140% hydration level: 1) a preparatory phase that is 20% of the total hatch time; 2) a pre-emergence development (reversible) phase that lasts for 50% of the total hatch time; and 3) a non-reversible phase that lasts for approximately 30% of the total hatch time [150]. Specific details of cellular activities at each stage are mentioned elsewhere [150].

Fig. 3.5 shows the differential impedance magnitude (Ω) of the brine shrimp cysts prior to hatching. Zero hours represent the time when the cysts were initially deposited into the saline solution. There was a measured increase of impedance from zero hours to the second data point at 1.4 hours which corresponds to the hydrating phase of the cysts. A hydrated cyst will have a higher reactance compared to the same cyst when dehydrated [151].

The change in differential impedance magnitude measured in the non-reversible phase corresponds to an increase of water content in the cysts. At the end of this phase, the osmotic pressure inside the cysts increases to a critical level, resulting in the breaking of the cyst shell. Figs. 3.5a, 3.5b, and 3.5c correspond to different cysts, however similar trends of impedance changes over time suggest this method is suitable for monitoring cyst development.

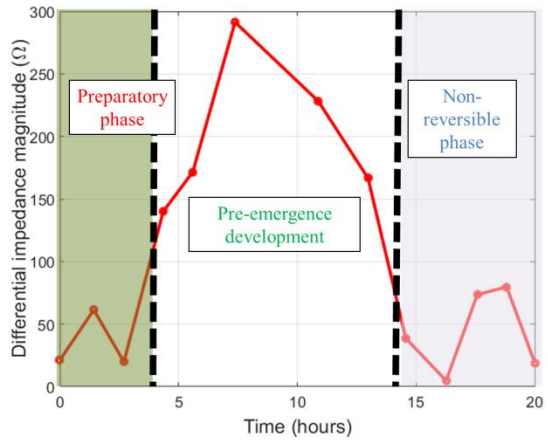

a

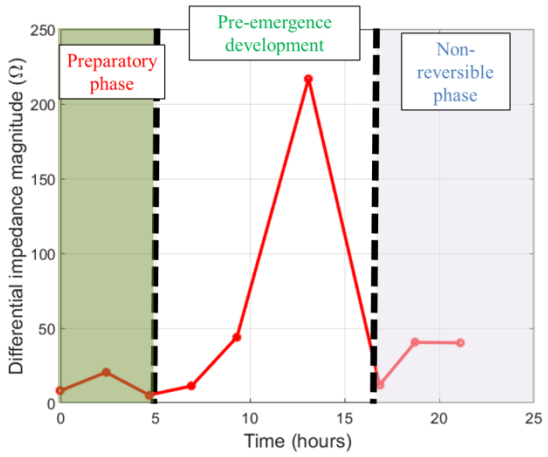

b

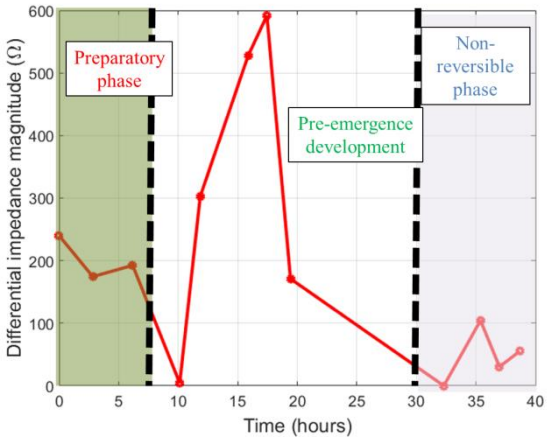

c

Figure 3.5: The results for impedance measurements correlating to major phases of cyst development. Differential impedance magnitude from 0 hours (when the cyst was first placed in media) until the approximate hatching time, for three separate cysts, adapted from [136]. The three major stages of development are outlined: the preparatory phase, the pre-emergence development phase, and the non-reversible phase.

3.7 DISCUSSION

The trend from the plots in Fig. 5 is that in the preparatory phase there is a low impedance which corresponds to a change in biological activity for the cyst, in the pre-emergence phase a large increase in impedance refers to another change in biological activity, and finally in the non-reversible phase there is a significant decrease in impedance which means another biological event has happened. Specifically, these events are marked through hydration of the cyst, ending the quiescence period and leading up to full hydration of the cyst, and finally hatching. The non-reversible phase indicates the end of dormancy, and if the cyst does not hatch then it will die. Three separate cysts had peak impedances in the preparatory, pre-emergence development, and non-reversible phases of 75 Ω, 300 Ω, and 100 Ω for the first cyst, 25 Ω, 225 Ω, and 50 Ω for the second cyst, and 250 Ω, 600 Ω, and 100 Ω for the third cyst.

A major concern was to also not severely impact the health of the *Artemia* cyst by interrogating it with electrical impulses. The effects of electric fields were previously investigated for freely swimming *Artemia,* and it was found that they could withstand 100 50-ns pulses of a 7 kV/cm field, 10 50-ns pulses of a 12 kV/cm field, and 2 50-ns pulses of a 20 kV/cm field before being immobilized [152]. The interrogation voltage in the experiments performed here is 1 V across a 500-μm gap, corresponding to an electric field of 20 V/cm, although the cysts are exposed to this electric field for a longer period than the higher fields tested in [152]. For the 17 other embryos that hatched in this study, 10% hatched within a day (less than 16 hours), 15% hatched within the experiment duration (24 to 72 hours, however did not yield similar impedance trends), 30% hatched after the experiment finished (more than 72 hours), and 40% did not hatch at all.

CHAPTER 4 CONCLUSION AND FUTURE WORK

Gene delivery was achieved for the placenta based plasmid constructs presented in this paper. The plan for optimizing these experiments allowed the use of previously proven constructs to verify the new plasmids for each experiment which included pGL3, Ept1, and Glut1.

Impedance changes during the development of *Artemia* cysts were presented in this paper. The cysts went through three phases: the preparatory phase, pre-emergence development phase, and the non-reversible phase. The peak impedances were found to be measured within the pre-emergence development phase, and are likely attributed with embryo activity in preparation for hatching from the cysts. These results show the feasibility of using impedance spectroscopy to measure activity in a hatching cyst.

In the current setup, the cyst is relatively small to the dimensions of both the microfluidic channel as well as the electrodes used. Reducing the channel size and increasing the electrode size relative to the size of the cyst can help to increase the signal-to-noise-ratio of the measurement. Further improvements on channel design as well as an automated data acquisition will also help to improve the quality of future tests.

APPENDIX

A. Matlab Executable titled SSD

```
%
%   SSD Code for communicating with an instrument.
%
%   This is the machine generated representation of an instrument control
%   session using a device object. The instrument control session comprises
%   all the steps you are likely to take when communicating with your
%   instrument. These steps are:
%
%       1. Create a device object
%       2. Connect to the instrument
%       3. Configure properties
%       4. Invoke functions
%       5. Disconnect from the instrument
%
%   To run the instrument control session, type the name of the file,
%   SSD, at the MATLAB command prompt.
%
%   The file, SSD must be on your MATLAB PATH. For additional information
%   on setting your MATLAB PATH, type 'help addpath' at the MATLAB command
%   prompt.
%
%   Example:
%       SSD;
%
%   See also ICDEVICE.
%

%   Creation time: 22-Dec-2015 14:55:12

%To open up matlab instrumentation toolbox type in the following
%tmtool

clear all
close all
clc

% Initialize variables
h = [1:2500]';
k = [];
pressh = [];%MPa
sensh = 89/1000;% V/MPa
mxh = [];% mVpp
```

```
mnh = [];% mVpp
hloops = 7;
hdata = [];

% htime are approximate times the waveforms were taken at.
htime = [];

for a = 1:hloops
  htime(a) = 1.7*a;
end

htime = htime';

% Create a VISA-USB object.
interfaceObj = instrfind('Type', 'visa-usb', 'RsrcName',
'USB0::0x0699::0x03B3::C010413::0::INSTR', 'Tag', '');

% Create the VISA-USB object if it does not exist
% otherwise use the object that was found.
if isempty(interfaceObj)
  interfaceObj = visa('NI', 'USB0::0x0699::0x03B3::C010413::0::INSTR');
else
  fclose(interfaceObj);
  interfaceObj = interfaceObj(1);
end

% Create a device object.
deviceObj = icdevice('tektronix_tds2024.mdd', interfaceObj);

% Connect device object to hardware.
connect(deviceObj);

% Execute device object function(s).
% The first for loop enables the capturing of multiple waveforms, with a
% period of 1.7 seconds per capture.
%   Concatenate h so we have ld columns of 2500 points.
%   h and k are y (time points) and x (pressure outputs) coordinates from the
oscilloscope, respectively.
groupObj = get(deviceObj, 'Waveform');

tic
for ld = 1:hloops
  [y,x] = invoke(groupObj, 'readwaveform', 'channel1');
  h = [h, y'];
  k = [k, x'];
end
```

```
toc

% Delete objects.
delete([deviceObj interfaceObj]);

% We convert the raw data into pressure outputs.
mxh = max(h);
mnh = min(h);
pressh = (abs(mxh - mnh)/sensh)';

% To write to an excel file use the xlswrite command.
% We will store both the raw data as well as the pressure converted data.
header = {'Time','700 mVpp Input'};
hdata = [htime,pressh(2:hloops+1)];

% Store raw data.
xlswrite('700 mVpp PW Input Olympus Focused Transducer raw data', h,1)
xlswrite('700 mVpp PW Input Olympus Focused Transducer raw data', k,2)

% Store pressure data.
xlswrite('700 mVpp PW Input Olympus Focused Transducer Pressure data in MPa',
header,1)
xlswrite('700 mVpp PW Input Olympus Focused Transducer Pressure data in MPa',
hdata,1, 'A2')

% Storing data from oscilloscope directly hooked up with amplifier.

% We convert the raw data into a max and min voltage.
mxh = max(h);
mnh = min(h);
pressh = (abs(mxh - mnh)/sensh)';

% To write to an excel file use the xlswrite command.
% We will store both the raw data as well as the pressure converted data.
header = {'Time','700 mVpp Input'};
hdata = [htime,pressh(2:hloops+1)];

% Store raw data.
xlswrite('700 mVpp PW Input Olympus Focused Transducer raw data', h,1)
xlswrite('700 mVpp PW Input Olympus Focused Transducer raw data', k,2)

% Store pressure data.
xlswrite('700 mVpp PW Input Olympus Focused Transducer Pressure data in MPa',
header,1)
xlswrite('700 mVpp PW Input Olympus Focused Transducer Pressure data in MPa',
hdata,1, 'A2')
```

BIBLIOGRAPHY

[1] Elsevier, "Developmental Biology," 2017. [Online]. Available: https://www.journals.elsevier.com/developmental-biology/. [Accessed July 2017].

[2] K. Elder and B. Dale, "In Vitro Fertilization," Cambridge, Cambridge University Press, 2000.

[3] D. G. Mitchell and M. Cohen, "MRI Principles," Philadelphia, Saunders, 2004.

[4] K. A. Ellenbogen, B. L. Wilkoff, N. Kay, C.-P. Lau and A. Auricchio, "Clinical Cardiac Pacing, Defibrillation and Resynchronization Therapy, Fifth Edition," Philadelphia, Elsevier, 2017.

[5] B. W. Orenstein, "Radiology Today," 1 December 2008. [Online]. Available: http://www.radiologytoday.net/archive/rt_120108p28.shtml. [Accessed July 2017].

[6] National Institude of Diabetes and Digestive and Kidney Diseases, "Overweight & Obesity Statistics," October 2012. [Online]. Available: https://www.niddk.nih.gov/health-information/health-statistics/overweight-obesity. [Accessed 2017].

[7] C. L. Ogden, M. D. Carroll, C. D. Fryar and K. M. Flegal, "Prevalence of Obesity Among Adults and Youth: United States, 2011-2014," National Center for Health Statistics, Hyattsville, 2015.

[8] The American College of Obstetricians and Gynecologists, "Obesity and Pregnancy," April 2016. [Online]. Available: https://www.acog.org/Patients/FAQs/Obesity-and-Pregnancy. [Accessed July 2017].

[9] S. Roan, "Package Deal," December 2015. [Online]. Available: http://magazine.uclahealth.org/body.cfm?id=6&action=detail&ref=1177. [Accessed July 2017].

[10] Centers for Disease Control and Prevention, "Strategies to Prevent Obesity," 27 October 2015. [Online]. Available: https://www.cdc.gov/obesity/strategies/index.html. [Accessed July 2017].

[11] Obesity Action Coalition, "Bariatric Surgery and Devices (Obesity, Severe Obesity)," 2017. [Online]. Available: http://www.obesityaction.org/obesity-treatments/bariatric-surgery.

[12] National Intitutes of Health, "Adeno-Associated Virus Gene Therapy for Diabetes and Obesity," 6 December 2016. [Online]. Available: https://www.ott.nih.gov/technology/e-142-2011 . [Accessed July 2017].

[13] B. P. Luscher, C. Marini, M. S. Joerger-Messerli, X. Huang, M. A. Hediger, C. Albrecht, M. U. Baurmann and D. V. Surbek, "Placental Glucose Transporter (GLUT)-1 is Down-Regulated in Preeclampsia," *Placenta*, vol. 55, pp. 94-99, 2017.

[14] your genome, "Why use the mouse in research?," Welcome Genome Campus, 3 March 2017. [Online]. Available: www.yourgenome.org/facts/why-use-the-mouse-in-research. [Accessed July 2017].

[15] National Human Genome, "Why Mouse Matters," 23 July 2010. [Online]. Available: https://www.genome.gov/10001345/importance-of-mouse-genome/. [Accessed July 2017].

[16] University of Kentucky, "Commonly Used Mouse Strains," [Online]. Available: https://www.research.uky.edu/dlar/documents/CommonMouseResearchModels.pdf. [Accessed July 2017].

[17] J. Mu, J. C. Slevin, D. Qu, S. McCormick and S. L. Adamson, "In vivo quantification of embryonic and placental growth during gestation in mice using micro-ultrasound," *Reproductive Biology Endocrinology*, vol. 6, no. 34, 2008.

[18] NDT Resource Center, "Basic Principles of Ultrasonic Testing," [Online]. Available: https://www.nde-ed.org/EducationResources/CommunityCollege/Ultrasonics/Introduction/description.htm. [Accessed July 2017].

[19] M. Postema, Fundamentals of Medical Ultrasonics, New York: Spon Press, 2011.

[20] F. Calliada, R. Campani, O. Bottinelli, A. Bozzini and M. G. Sommaruga, "Ultrasound Contrast Agents Basic Principles," *European Journal of Radiology,* vol. 27, pp. S157-S160, 1998.

[21] R. Taylor and J. S. Schultz, Handbook of Chemical and Biological Sensors, Philadelphia: Institute of Physics Publishing, 1996, pp. 11-15.

[22] M. Kleiner, Acoustics and Audio Technology, Fort Lauderdale, FL: J. Ross Publishing, 2012, pp. 8-9.

[23] M. F. Iskander, Electromagnetic Fields and Waves, Long Grove: Waveland Press, 1992.

[24] H. Azhari, Basics of Biomedical Ultrasound for Engineers, Wiley-IEEE Press, 2010, pp. 313-314.

[25] C. Holland and J. Fowlkes, Biological Effects and Safety, C. Rumack, S. Wilson and J. Charboneau, Eds., Mosby: Elsevier, 2011, pp. 34-52.

[26] F. Duck, "Medical and Non-Medical Protection Standards for Ultrasound and Infrasound," *Progress in Biophysics and Molecular Biology,* vol. 93, no. 1-3, pp. 176-191, 2007.

[27] Ghent University, "Ine De Cock," 2017. [Online]. Available: https://www.ugent.be/fw/pharmaceutics/biochemphypharm/en/team/inedc.htm. [Accessed July 2017].

[28] Scitable, "plasmid/plasmids," Nature Education, 2014. [Online]. Available: https://www.nature.com/scitable/definition/plasmid-plasmids-28. [Accessed July 2017].

[29] addgene, "Tetracycline (Tet) Inducible Expression," [Online]. Available: https://www.addgene.org/tetracycline/. [Accessed July 2017].

[30] C. Anderson, J. Urschitz, M. Khemmani, J. Owens, S. Moisyadi and R. Shohet, "Ultrasound Directs a Transposase System for Durable Hepatic Gene Delivery in Mice," *Ultrasound in Medicine & Biology,* vol. 39, no. 12, pp. 2351-2361, 2013.

[31] S. Keegan, J. Arellano and T. Gruner, "Validating the Measurement of Red Blood Cell Diameter in Fresh Capillary Blood by Darkfield Microscopy: A Pilot Study," *Advances in Integrative Medicine,* vol. 3, no. 1, pp. 11-14, 2016.

[32] The Oxford Companion to the Body, Blood Vessels, Oxford: Oxford University Press, 2001.

[33] S. Sirsi and M. Borden, "Microbubble Compositions, Properties and Biomedical Applications," *Bubble Science Engineering & Technology,* vol. 1, pp. 3-17, 2009.

[34] H. Li, X. Zheng, H. Wang, F. Li, Y. Wu and L. Du, "Ultrasound-Targeted Microbubble Destruction Enhances AAV-Mediated Gene Transfection in Human RPE Cells In Vitro and Rat Retina In Vivo," *Gene Therapy,* vol. 16, pp. 1146-1153, 2009.

[35] J. Lindner, "Microbubbles in Medical Imaging: Current Applications and Future Directions," *Nature Reviews Drug Discovery,* vol. 3, pp. 527-532, 2004.

[36] C. Walton, C. Anderson, R. Boulay and R. Shohet, "Introduction to the Ultrasound Targeted Microbubble Destruction Technique," *Journal of Visualized Experiments,* 12 June 2011.

[37] Z. Shen, A. Brayman, L. Chen and C. Miao, "Ultrasound with Microbubbles Enhances Gene Expression of Plasmid DNA in the Liver via Intraportal Delivery," *Gene Therapy,* vol. 15, no. 16, pp. 1147-1155, 2008.

[38] S. Song, Z. Shen, A. Brayman and C. Miao, "Explorations of High-Intensity Therapeutic Ultrasound and Microbubble-Mediated Gene Delivery in Mouse Liver," *Gene Therapy,* vol. 18, no. 10, pp. 1006-1014, 2011.

[39] R. Ishida, D. Kami, T. Kusaba, Y. Kirita, T. Kishida, O. Mazda, T. Adachi and S. Gojo, "Kidney-Specific Sonoporation-Mediated Gene Transfer," *Molecular Therapy,* vol. 24, no. 1, pp. 125-134, 2016.

[40] J. Lin, F. Li, H. Wang, F. Wei, P. Qin and L. Du, "Ultrasound Targeted Microbubble Destruction Stimulates Cellular Endocytosis in Facilitation of Adeno-Associated Virus Delivery," *International Journal of Molecular Sciences,* vol. 14, no. 5, pp. 9737-9750, 2013.

[41] X. Zheng, P. Ji and J. Hu, "Sonoporation Using Microbubbles Promotes Lipofectamine-Mediated siRNA Transduction to Rat Retina," *Bosnian Journal of Basic Medical Sciences,* vol. 11, no. 3, pp. 147-152, 2011.

[42] P. P. Sanches, M. Muelmeister, R. Seip, E. Kaijzel, C. Löwik, M. Boehmer, K. Tiemann and H. H. Grüll, "Ultrasound-Mediated Gene Delivery of Naked Plasmid DNA in Skeletal Muscles: A Case for Bolus Injections," *Journal of Controlled Release,* vol. 195, pp. 130-137, 2014.

[43] C. Fan, C. Ting, H. Liu, C. Huang, H. Hsieh, T. Yen, K. Wei and C. Yeh, "Antiangiogenic-Targeting Drug-Loaded Microbubbles Combined with Focused Ultrasound for Glioma Treatment," *Biomaterials,* vol. 34, no. 8, pp. 2142-2155, 2013.

[44] Y. Teng, M. Bai, Y. Sun, Q. Wang, F. Li, J. Xing, L. Du, T. Gong and Y. Duan, "Enhanced Delivery of PEAL Nanoparticles with Ultrasound Targeted Microbubble Destruction Mediated siRNA Transfection in Human MCF-7/S and MCF-7/ADR Cells In Vitro," *International Journal of Nanomedicine,* vol. 10, pp. 5447-5457, 2015.

[45] A. Carson, C. Mctiernan, L. Lavery, A. Hodnick, M. Grata, X. Leng, J. Wang, X. Chen, R. Modzelewski and F. Villanueva, "Gene Therapy of Carcinoma Using Ultrasound-Targeted Microbubble Destruction," *Ultrasound in Medicine and Biology,* vol. 37, no. 3, pp. 393-402, 2011.

[46] S. Rizzitelli, P. Giustetto, J. Cutrin, D. Castelli, C. Boffa, M. Ruzza, V. Menchise, F. Molinari, S. Aime and E. Terreno, "Sonosensitive Theranostic Liposomes for Preclinical In Vivo MRI-Guided Visualization of Doxorubicin Release Stimulated by Pulsed Low Intensity Non-Focused Ultrasound," *Journal of Controlled Release,* vol. 202, pp. 21-30, 2015.

[47] S. Rizzitelli, P. Giustetto, D. Faletto, D. Castelli, S. Aime and E. Terreno, "The Release of Doxorubicin From Liposomes Monitored by MRI and Triggered by a Combination of US Stimuli Led to a Complete Tumor Regression in a Breast Cancer Mouse Model," *Journal of Controlled Release,* vol. 230, pp. 57-63, 2016.

[48] Y. Zhao, Q. Lin, H. Wong, X. Shen, W. Yang, H. Xu, K. Mao, F. Tian, J. Yang, J. Xu, J. Xiao and C. Lu, "Glioma-Targeted Therapy using Cilengitide Nanoparticles Combined with UTMD Enhanced Delivery," *Journal of Controlled Release,* vol. 224, pp. 112-125, 2016.

[49] L. Sun, C. Huang, J. Wu, K. Chen, S. Li, R. Weisel, H. Rakowski, H. Sung and R. Li, "The use of Cationic Microbubbles to Improve Ultrasound-Targeted Gene Delivery to the Ischemic Myocardium," *Biomaterials,* vol. 34, pp. 2107-2116, 2013.

[50] A. Xie, T. Belcik, Y. Qi, T. Morgan, S. Champaneri, S. Taylor, B. Davidson, Y. Zhao, A. Klibanov, M. Kuliszewski, H. Leong-Poi, A. Ammi and J. Lindner, "Ultrasound-Mediated Vascular Gene Transfection by Cavitation of Endothelial-Targeted Cationic Microbubbles," *Journal of the American College of Cardiology: Cardiovascular Imaging,* vol. 5, no. 12, pp. 1253-1262, 2012.

[51] A. Carson, C. Mctiernan, L. Lavery, M. Grata, X. Leng, J. Wang, X. Chen and F. Villanueva, "Ultrasound-Targeted Microbubble Destruction to Deliver siRNA Cancer Therapy," *Cancer Research,* vol. 72, no. 23, pp. 6191-6199, 2012.

[52] X. Jing, J. Liu, B. Yang, S. Fu, T. Wu and D. Wang, "EGFP Gene Transfection Into the Synovial Joint Tissues of Rats with Rheumatoid Arthritis by Ultrasound-Mediated Microbubble Destruction," *Experimental and Therapeutic Medicine,* vol. 7, no. 5, pp. 1396-1402, 2014.

[53] G. Shapiro, A. Wong, M. Bez, F. Yang, S. Tam, L. Even, D. Sheyn, S. Ben-David, W. Tawackoli, G. Pelled, K. Ferrara and D. Gazit, "Multiparameter Evaluation of In Vivo Gene Delivery Using Ultrasound-Guided, Microbubble-Enhanced Sonoporation," *Journal of Controlled Release,* vol. 223, pp. 157-164, 2016.

[54] S. Wu, C. Chen, Y. Tung, O. Olumolade and E. Konofagou, "Effects of the Microbubble Shell Physicochemical Properties on Ultrasound-Mediated Drug Delivery to the Brain," *Journal of Controlled Release,* vol. 212, pp. 30-40, 2015.

[55] D. Wang, C. Panje, M. Pysz, R. Paulmurugan, J. Rosenberg, S. Gambhir, M. Schneider and J. Willmann, "Cationic Versus Neutral Microbubbles for Ultrasound-Mediated Gene Delivery in Cancer," *Radiology,* vol. 264, pp. 721-732, 2012.

[56] S. Pislaru, C. Pislaru, R. Kinnick, R. Singh, R. Gulati, J. Greenleaf and R. Simari, "Optimization of Ultrasound-Mediated Gene Transfer-Comparison of Contrast Agents and Ultrasound Modalities," *European Heart Journal,* vol. 24, no. 18, pp. 1690-1698, 2003.

[57] J. Kobulnik, M. Kuliszewski, D. Stewart, J. Lindner and H. Leong-Poi, "Comparison of Gene Delivery Techniques for Therapeutic Angiogenesis: Ultrasound-Mediated Destruction of Carrier Microbubbles Versus Direct Intramuscular Injection.," *Journal of the American College of Cardiology,* vol. 54, no. 18, pp. 1735-1742, 2009.

[58] S. Chen, J. Ding, R. Bekeredjian, B. Yang, R. Shohet, S. Johnston, H. Hohmeier, C. Newgard and P. Grayburn, "Efficient Gene Delivery to Pancreatic Islets with Ultrasonic Microbubble Destruction Technology," *Proceedings of the National Academy of Sciences of the United States,* vol. 103, no. 22, pp. 8469-8474, 2006.

[59] Y. Anna, L. Matthieu, D. Mariska, L. Sander, G. Holger and M. Chrit, "In Vivo Temperature Controlled Ultrasound-Mediated Intracellular Delivery of Cell-Impermeable Compounds," *Journal of Controlled Release,* vol. 161, no. 1, pp. 90-97, 2012.

[60] C. Burke, J. Suk, A. Kim, Y. Hsiang, A. Klibanov, J. Hanes and R. Price, "Markedly Enhanced Skeletal Muscle Transfection Achieved by the Ultrasound-Targeted Delivery of Non-Viral Gene Nanocarriers with Microbubbles," *Journal of Controlled Release,* vol. 162, no. 2, pp. 414-421, 2012.

[61] Q. Hu, H. Liang, T. Partridge and M. Blomley, "Microbubble Ultrasound Improves the Efficiency of Gene Transduction in Skeletal Muscle In Vivo with Reduced Tissue Damage," *Gene Therapy,* vol. 10, no. 5, pp. 396-405, 2003.

[62] S. Sirsi, S. Hernandez, L. Zielinski, H. Blomback, A. Koubaa, M. Synder, S. Homma, J. Kandel, D. Yamashiro and M. Borden, "Polyplex-Microbubble Hybrids for Ultrasound-Guided Plasmid DNA Delivery to Solid Tumors," *Journal of Controlled Release,* vol. 157, no. 2, pp. 224-234, 2012.

[63] C. Yoon, H. Jung, M. Kown, S. Lee, C. Kim, M. Kim, M. Lee and J. Park, "Sonoporation of the Minicircle-VEGF for Wound Healing of Diabetic Mice," *Pharmaceutical Research,* vol. 26, no. 4, pp. 794-801, 2009.

[64] A. Smith, M. Kuliszewski, C. Liao, D. Rudenko, D. Stewart and H. Leong-Poi, "Sustained Improvement in Perfusion and Flow Reserve After Temporally Separated Delivery of Vascular Endothelial Growth Factor and Angiopoietin-1 Plasmid Deoxyribonucleic Acid," *Journal of the American College of Cardiology,* vol. 59, no. 14, pp. 1320-1328, 2012.

[65] Y. Liu, H. Miyoshi and M. Nakamura, "Targeted Vascular Delivery of Antisense Molecules using Intravenous Microbubbles," *Journal of Controlled Release,* vol. 114, no. 1, pp. 89-99, 2016.

[66] H. Leong-Poi, M. Kuliszewski, M. Lekas, M. Sibbald, K. Teichert-Kuliszewska, A. Kibanov, D. Stewart and J. Lindner, "Therapeutic Arteriogenesis by Ultrasound-Mediated VEGF Plasmid Gene Delivery to Chronically Ischemic Skeletal Muscle," *Circulation Research,* vol. 101, no. 3, pp. 295-303, 2007.

[67] K. Anwer, G. Kao, B. Proctor, I. Anscombe, V. Florack, R. Earls, E. Wilson, T. McCreery, E. Unger, A. Rolland and S. Sullivan, "Ultrasound Enhancement of Cationic Lipid-Mediated Gene Transfer to Primary Tumors Following Systemic Administration," *Gene Therapy,* vol. 7, no. 21, pp. 1833-1839, 2000.

[68] P. Li, Y. Zheng, H. Ran, J. Tan, Y. Lin, Q. Zhang, J. Ren and Z. Wang, "Ultrasound Triggered Drug Release from 10-Hydroxycamptothecin-Loaded Phospholipid Microbubbles for Targeted Tumor Therapy in Mice," *Journal of Controlled Release,* vol. 162, no. 2, pp. 349-354, 2012.

[69] C. Panje, D. Wang, M. Pysz, R. Paulmurugan, Y. Ren, F. Tranquart, L. Tian and J. Willmann, "Ultrasound-Mediated Gene Delivery with Cationic Versus Neutral Microbubbles: Effect of DNA and Microbubble Dose on In Vivo Transfection Efficiency," *Theranostics,* vol. 2, no. 11, pp. 1078-1091, 2012.

[70] H. Fujii, Z. Sun, S. Li, J. Wu, S. Fazel, R. Weisel, H. Rakowski, J. Lindner and R. Li, "Ultrasound-Targeted Gene Delivery Induces Angiogenesis After a Myocardial Infarction in Mice," *Journal of the American College of Cardiology: Cardiovascular Imaging,* vol. 2, no. 7, pp. 869-879, 2009.

[71] O. Muller, S. Schinkel, J. Kleinschmidt, H. Katus and R. Bekeredjian, "Augmentation of AAV-Mediated Cardiac Gene Transferafter Systemic Administration in Adult Rats," *Gene Therapy,* vol. 15, no. 23, pp. 1558-1565, 2008.

[72] Y. Negishi, Y. Endo, T. Fukuyama, R. Suzuki, T. Takizawa, D. Omata, K. Maruyama and Y. Aramaki, "Delivery of siRNA into the Cytoplasm by Liposomal Bubbles and Ultrasound," *Journal of Controlled Release,* vol. 132, no. 2, pp. 124-130, 2008.

[73] K. Un, S. Kawakami, R. Suzuki, K. Maruyama, F. Yamashita and M. Hashida, "Development of an Ultrasound-Responsive and Mannose-Modified Gene Carrier for DNA Vaccine Therapy," *Biomaterials,* vol. 31, no. 30, pp. 7813-7826, 2010.

[74] S. Chen, J. Chen, P. Huang, X. Meng, S. Clayton, J. Shen and P. Grayburn, "Myocardial Regeneration in Adriamycin Cardiomyopathy by Nuclear Expression of GLP1 using Ultrasound Targeted Microbubble Destruction," *Biochemical and Biophysical Research Communications,* vol. 458, no. 4, pp. 823-829, 2015.

[75] S. Chen, M. Shimoda, J. Chen and P. Grayburn, "Stimulation of Adult Resident Cardiac Progenitor Cells by Durable Myocardial Expression of Thymosin Beta 4 with Ultrasound-Targeted Microbubble Delivery," *Gene Therapy,* vol. 20, no. 2, pp. 225-233, 2013.

[76] J. Chen, S. Chen, P. Huang, X. Meng, S. Clayton, J. Shen and P. Grayburn, "In Vivo Targeted Delivery of ANGPTL8 Gene for Beta Cell Regeneration in Rats," *Diabetologia,* vol. 58, no. 5, pp. 1036-1044, 2015.

[77] S. Chen, R. Shohet, R. Bekeredjian, P. Frenkel and P. Grayburn, "Optimization of Ultrasound Parameters for Cardiac Gene Delivery of Adenoviral or Plasmid Deoxyribonucleic Acid by Ultrasound-Targeted Microbubble Destruction," *Journal of the American College of Cardiology,* vol. 42, no. 2, pp. 301-308, 2003.

[78] R. Bekeredjian, S. Chen, P. Frenkel, P. Grayburn and R. Shohet, "Ultrasound-Targeted Microbubble Destruction can Repeatedly Direct Highly Specific Plasmid Expression to the Heart," *Circulation,* vol. 108, no. 8, pp. 1022-1026, 2003.

[79] K. Wei, D. Skyba, C. Firschke, A. Jayaweera, J. Lindner and S. Kaul, "Interactions Between Microbubbles and Ultrasound: In Vitro and In Vivo Observations," *Journal of the American College of Cardiology,* vol. 29, no. 5, 1997.

[80] R. Suzuki, T. Takizawa, Y. Negishi, N. Utoguchi and K. Maruyama, "Effective Gene Delivery with Novel Liposomal Bubbles and Ultrasonic Destruction Technology," *International Journal of Pharmaceutics,* vol. 354, pp. 49-55, 2008.

[81] Y. Endo-Takahashi, Y. Negishi, A. Nakamura, D. Suzuki, S. Ukai, K. Sugimoto, F. Moriyasu, N. Takagi, R. Suzuki, K. Maruyama and Y. Aramaki, "pDNA-Loaded Bubble Liposomes as Potential Ultrasound Imaging and Gene Delivery Agents," *Biomaterials,* vol. 34, no. 11, pp. 2807-2813, 2013.

[82] N. Geis, C. Mayer, R. Kroll, S. Hardt, H. Katus and R. Bekeredjian, "Spatial Distribution of Ultrasound Targeted Microbubble Destruction Increases Cardiac Transgene Expression but not Capillary Permeability," *Ultrasound in Medicine and Biology,* vol. 35, pp. 1119-1126, 2009.

[83] I. Kondo, K. Ohmori, A. Oshita, H. Takeuchi, S. Fuke, K. Shinomiya, T. Noma, T. Namba and M. Kohno, "Treatment of Acute Myocardial Infarction by Hepatocyte Growth Factor Gene Transfer: The First Demonstration of Myocardial Transfer of a "Functional" Gene using Ultrasonic Microbubble Destruction," *Journal of the American College of Cardiology,* vol. 44, pp. 644-653, 2004.

[84] J. Tlaxca, J. Rychak, P. Ernst, P. Konkalmatt, T. Shevchenko, T. Pizarro, J. Rivera-Nieves, A. Klibanov and M. Lawrence, "Ultrasound-Based Molecular Imaging and Specific Gene Delivery to Mesenteric Vasculature by Endothelial Adhesion Molecule Targeted Microbubbles in a Mouse Model of Crohn's Disease," *Journal of Controlled Release,* vol. 165, pp. 216-225, 2013.

[85] A. Carson, C. McTiernan, L. Lavery, A. Hodnick, M. Grata, X. Leng, J. Wang, X. Chen, R. Modzelewski and F. Villanueva, "Gene Therapy of Carcinoma Using Ultrasound-Targeted Microbubble Destruction," *Ultrasound in Medicine and Biology,* vol. 37, pp. 393-402, 2011.

[86] B. Chertok, R. Langer and D. Anderson, "Spatial Control of Gene Expression by Nanocarriers Using Heparin Masking and Ultrasound-Targeted Microbubble Destruction," *ACS Nano,* vol. 10, pp. 7267-7278, 2016.

[87] M. Cochran, J. Eisenbrey, M. Soulen, S. Schultz, R. Ouma, S. White, E. Furth and M. Wheatley, "Disposition of Ultrasound Sensitive Polymeric Drug Carrier in a Rat Hepatocullular Carcinoa Model," *Academic Radiology,* vol. 18, pp. 1341-1348, 2011.

[88] Y. Ji, Z. Han, L. Shao and Y. Zhao, "Evaluation of In Vivo Antitumor Effects of Low- Frequency Ultrasound-Mediated miRNA- 133a Microbubble Delivery in Breast Cancer," *Cancer Medicine,* vol. 5, pp. 2534-2543, 2016.

[89] T. Rooij, I. Skachkov, I. Beekers, K. Lattwein, J. Voorneveld, T. Kokhuis, D. Bera, Y. Luan, A. Steen, N. Jong and K. Kooiman, "Viability of Endothelial Cells after Ultrasound-Mediated Sonoporation: Influence of Targeting, Oscillation, and Displacement of Microbubbles," *Journal of Controlled Release,* vol. 238, pp. 197-211, 2016.

[90] M. Tamosiunas, R. Kadikis, I. Saknite, J. Baltusnikas, A. Kilikevicius, A. Lihachev, R. Petrovska, D. Jakovels and S. Satkauskas, "Noninvasive Optical Diagnostics of Enhanced Green Fluorescent Protein Expression in Skeletal Muscle for Comparison of Electroporation and Sonoporation Efficiencies," *Journal of Biomedical Optics,* vol. 21, 2016.

[91] Y. Bae, Y. Yoon, T. Yoon and H. Lee, "Ultrasound-Guided Delivery of siRNA and a Chemotherapeutic Drug by Using Microbubble Complexes: In Vitro and In Vivo Evaluations in a Prostate Cancer Model," *Korean Journal of Radiology,* vol. 17, pp. 497-508, 2016.

[92] T. Wang, J. Choe, K. Pu, R. Devulapally, S. Bachawal, S. Machtaler, S. Chowdhury, R. Luong, L. Tian, B. Khuri-Yakub, J. Rao, R. Paulmurugan and J. Willmann, "Ultrasound-Guided Delivery of microRNA Loaded Nanoparticles into Cancer," *Journal of Controlled Release,* vol. 203, pp. 99-108, 2015.

[93] S. Kato, S. Mori and T. Kodama, "A Novel Treatment Method for Lymph Node Metastasis Using a Lymphatic Drug Delivery System with Nano/Microbubbles and Ultrasound," *Journal of Cancer,* vol. 6, pp. 1282-1294, 2015.

[94] J. Castle, K. Kent, Y. Fan, K. Wallace, C. Davis, J. Roberts, M. Marino, K. Thomenius, H. Lim, E. Coles, M. Davidson, S. Feinstein and A. DeMaria, "Therapeutic Ultrasound: Increased HDL-Cholesterol Following Infusions of Acoustic Microspheres and Apolipoprotein A-I Plasmids," *Atherosclerosis,* vol. 241, pp. 92-99, 2015.

[95] S. Okunaga, A. Takasu, N. Meshii, T. Imai, M. Hamada, S. Iwai and Y. Yura, "Ultrasound as a Method to Enhance Antitumor Ability of Oncolytic Herpes Simplex Virus for Head and Neck Cancer," *Cancer Gene Therapy*, vol. 22, pp. 163-168, 2015.

[96] R. Geguchadze, Z. Wang, L. Zourelias, P. Perez-Riveros, P. Edwards, L. Machen and M. Passineau, "Proteomic Profiling of Salivary Gland After Nonviral Gene Transfer Mediated by Conventional Plasmids and Minicircles," *Molecular Therapy Methods and Clinical Development*, vol. 1, 2014.

[97] Y. Yoon, Y. Kswon, H. Cho, S. Heo, K. Park, S. Park, S. Lee, S. Hwang, Y. Kim, H. Jae, G. Ahn, Y. Cho, H. Lee, H. Lee and T. Yoon, "Ultrasound-Mediated Gene and Drug Delivery Using a Microbubble-Liposome Particle System," *Theranostics*, vol. 4, pp. 1133-1144, 2014.

[98] T. Kurosaki, S. Kawakami, Y. Higuchi, R. Suzuki, K. Maruyama, H. Sasaki, F. Yamashita and M. Hashida, "Kidney-Selective Gene Transfection Using Anionic Bubble Lipopolyplexes with Renal Ultrasound Irradiation in Mice," *Nanomedicine*, vol. 10, pp. 1829-1838, 2014.

[99] Y. Kono, S. Kawakami, Y. Higuchi, K. Maruyama, F. Yamashita and M. Hashida, "Antitumor Effect of Nuclear Factor-κB Decoy Transfer by Mannose-Modified Bubble Lipoplex into Macrophages in Mouse Malignant Ascites," *Cancer Science*, vol. 105, pp. 1049-1055, 2014.

[100] T. Sato, S. Mori, Y. Arai and T. Kodama, "The Combination of Intralymphatic Chemotherapy With Ultrasound and Nano-/Microbubbles Is Efficient in the Treatment of Experimental Tumors in Mouse Lymph Nodes," *Ultrasound in Medicine and Biology*, vol. 40, pp. 1237-1249, 2014.

[101] R. Sun, M. Noble, S. Sun, S. Song and C. Miao, "Development of Therapeutic Microbubbles for Enhancing Ultrasound-Mediated Gene Delivery," *Journal of Controlled Release*, vol. 182, pp. 111-120, 2014.

[102] Y. Kono, S. Kawakami, Y. Higuchi, K. Maruyama, F. Yamashita and M. Hashida, "Tumour-Associated Macrophages Targeted Transfection with NF-kB Decoy/Mannose-Modified Bubble Lipoplexes Inhibits Tumour Growth in Tumour-Bearing Mice," *Journal of Drug Targeting*, vol. 22, pp. 439-449, 2014.

[103] N. Yamatomo, T. Iwagami, I. Kato, S. Masunaga, Y. Sakurai, S. Iwai, M. Nakazawa, K. Ono and Y. Yura, "Sonoporation as an Enhancing Method for Boron Neutron Capture Therapy for Squamous Cell Carcinomas," *Radioation Oncology*, vol. 8, p. 280, 2013.

[104] H. Inoue, Y. Arai, T. Kishida, M. Shin-Ya, R. Terauchi, S. Nakagawa, M. Saito, S. Tsuchida, A. Inoue, T. Shirai, H. Fujiwara, O. Mazda and T. Kubo, "Sonoporation-Mediated Transduction of siRNA Ameliorated Experimental Arthritis using 3 MHz Pulsed Ultrasound," *Ultrasonics*, vol. 54, pp. 874-881, 2014.

[105] G. Feichtinger, A. Hofmann, P. Slezak, S. Schuetzenberger, M. Kaipel, E. Schwartz, A. Neef, N. Nomikou, T. Nau, M. Griensven, A. McHale and H. Redl, "Sonoporation Increases Therapeutic Efficacy of Inducible and Constitutive BMP2/7 In Vivo Gene Delivery," *Human Gene Therapy Methods*, vol. 25, pp. 57-71, 2014.

[106] L. Luo, F. Wu, B. Wang, T. Xu, J. Hu and S. Y. , "Optimization of Acoustic Parameters of Microbubble-Enhanced Ultrasound Sonoporation for Augmenting Tumor Cell Permeability In Vivo," *Journal of Southern Medical University*, vol. 33, pp. 1377-1381, 2013.

[107] O. Zolochevska, J. Ellis, S. Parlkar, D. Chan-Seng, T. Emrick, J. Wei, I. Patrikeev, M. Motamedi and M. Figueiredo, "Interleukin-27 Gene Delivery for Modifying Malignant Interactions Between Prostate Tumor and Bone," *Human Gene Therapy*, vol. 24, pp. 970-981, 2013.

[108] S. Kotopoulis, G. Dimcevski, O. Gilja, D. Hoem and M. Postema, "Treatment of Human Pancreatic Cancer using Combined Ultrasound, Microbubbles, and Gemcitabine: A Clinical Case Study," *Medical Physics*, vol. 40, p. 072902, 2013.

[109] J. Lee, C. Lo, S. Ka, A. Chen and W. Chen, "Prolonging the Expression Duration of Ultrasound-Mediated Gene Transfection using PEI Nanoparticles," *Journal of Controlled Release,* vol. 160, pp. 64-71, 2012.

[110] Z. Liao, K. Tsai, W. Wang, S. Tseng, W. Deng, W. Chen and L. Hwang, "Sonoporation-Mediated Anti-Angiogenic Gene Transfer into Muscle Effectively Regresses Distant Orthotopic Tumors," *Cancer Gene Therapy,* vol. 19, pp. 171-180, 2012.

[111] L. Kowalczuk, M. Boudinet, M. Sanharawi, E. Touchard, M. Naud, A. Saied, J. Jeanny, F. Behar-Cohen and P. Laugier, "In Vivo Gene Transfer into the Ocular Ciliary Muscle Mediated by Ultrasound and Microbubbles," *Ultrasound in Medicine and Biology,* vol. 37, pp. 1814-1827, 2011.

[112] J. Lemmon, R. McFarland, J. Rybicka, D. Balce, K. McKeown, R. Krohn, T. Matsunaga and R. Yates, "In Vitro and In Vivo Transfection of Primary Phagocytes via Microbubble-Mediated Intraphagosomal Sonoporation," *Journal of Immunological Methods,* vol. 371, pp. 152-158, 2011.

[113] H. Hasanzadeh, M. Mokhtari-Dizaji, S. Bathaie and Z. Hassan, "Effect of Local Dual Frequency Sonication on Drug Distribution From Polymeric Nanomicelles," *Ultrasonics Sonochemistry,* vol. 18, pp. 1165-1171, 2011.

[114] M. Matsuo, K. Yamaguchi, L. J. Feril, H. Endo, K. Ogawa, K. Tachibana and J. Nakayama, "Synergistic Inhibition of Malignant Melanoma Proliferation by Melphalan Combined with Ultrasound and Microbubbles," *Ultrasonics Sonochemistry,* vol. 18, pp. 1218-1224, 2011.

[115] Y. Chen, L. Jiang, N. Liu, L. Ding, X. Liu, Z. Wang, K. Hong and Q. Zhang, "Enhanced Gene Transduction into Skeletal Muscle of Mice In Vivo with Pluronic Block Copolymers and Ultrasound Exposure," *Cell Biochemistry and Biophysics,* vol. 60, pp. 267-273, 2011.

[116] T. Kodama, A. Aoi, Y. Watanabe, S. Horie, M. Kodama, L. Li, R. Chen, N. Teramoto, H. Morikawa, S. Mori and M. Fukumoto, "Evaluation of Transfection Efficiency in Skeletal Muscle using Nano/Microbubbles and Ultrasound," *Ultrasound in Medicine and Biology,* vol. 36, pp. 1196-1205, 2010.

[117] G. Casey, J. Cashman, D. Morrissey, M. Whelan, J. Larkin, D. Soden, M. Tangney and G. O'Sullivan, "Sonoporation Mediated Immunogene Therapy of Solid Tumors," *Ultrasound in Medicine and Biology,* vol. 36, pp. 430-440, 2010.

[118] S. Xenariou, H. Liang, U. Griesenbach, J. Zhu, R. Farley, L. Somerton, C. Singh, P. Jeffery, R. Scheule, S. Cheng, D. Geddes, M. Blomley and E. Alton, "Low-Frequency Ultrasound Increases Non-viral Gene Transfer to the Mouse Lung," *Acta Biochimica et Biophysica Sinica,* vol. 42, pp. 45-51, 2010.

[119] K. Tsai, Z. Liao, S. Yang, W. Lin, M. Shieh, L. Hwang and W. Chen, "Differences in Gene Expression Between Sonoporation in Tumor and in Muscle," *The Journal of Gene Medicine,* vol. 11, pp. 933-940, 2009.

[120] T. Sakai, M. Kawaguchi and Y. Ksuge, "siRNA-Mediated Gene Silencing in the Salivary Gland using In Vivo Microbubble-Enhanced Sonoporation," *Oral Diseases,* vol. 15, pp. 505-511, 2009.

[121] S. Hayashi, M. Mizuno, J. Yoshida and A. Nakao, "Effect of Sonoporation on Cationic Liposome-Mediated IFNbeta Gene Therapy for Metastatic Hepatic Tumors of Murine Colon Cancer," *Cancer Gene Therapy,* vol. 16, pp. 638-643, 2009.

[122] R. Suzuki, Y. Oda, E. Namai, T. Takizawa, Y. Negishi, N. Utoguchi, K. Tachibana and K. Maruyama, "Development of Site Specific Gene Delivery System with Sonoporation," *Yakugaku Zasshi,* vol. 128, pp. 187-192, 2008.

[123] D. Sheyn, N. Kimelman-Bleich, G. Pelled, Y. Zilberman, D. Gazit and Z. Gazit, "Ultrasound-Based Nonviral Gene Delivery Induces Bone Formation In Vivo," *Gene Therapy,* vol. 15, pp. 257-266, 2008.

[124] M. Saito, O. Mazda, K. Takahashi, Y. Arai, T. Kishida, M. Shin-Ya, A. Inoue, H. Tonomura, K. Sakao, T. Morihara, J. Imanishi, M. Kawata and T. Kubo, "Sonoporation Mediated Transduction of pDNA/siRNA into Joint Synovium In Vivo," *Journal of Orthopaedic Research,* vol. 25, pp. 1308-1316, 2007.

[125] K. Iwanaga, K. Tominaga, K. Yamamoto, M. Habu, H. Maeda, S. Akifusa, T. Tsujisawa, T. Okinaga, J. Fukuda and T. Nishihara, "Local Delivery System of Cytotoxic Agents to Tumors by Focused Sonoporation," *Cancer Gene Therapy,* vol. 14, pp. 354-363, 2007.

[126] S. Tsunoda, O. Mazda, Y. Oda, Y. Iida, S. Akabame, T. Kishida, M. Shin-Ya, H. Asada, S. Gojo, J. Imanishi, H. Matsubara and T. Yoshikawa, "Sonoporation using Microbubble BR14 Promotes pDNA/siRNA Transduction to Murine Heart," *Biochemistry and Biophysics Research Communications,* vol. 336, pp. 118-127, 2005.

[127] P. Hauff, S. Seemann, R. Reszka, M. Schultze-Mosgau, M. Reinhardt, T. Buzasi, T. Plath, S. Rosewicz and M. Schirner, "Evaluation of Gas-Filled Microparticles and Sonoporation as Gene Delivery System: Feasibility Study in Rodent Tumor Models," *Radiology,* vol. 236, pp. 572-578, 2005.

[128] L. Lei, Z. Liu, S. Ohta and G. Yamada, "In Vivo Transduction of EGFP into Female Mouse Reproductive System by Electroporation and Microbubble-Enhanced Sonoporation," *Journal of Molecular Cell Biology,* vol. 39, pp. 378-382, 2006.

[129] Y. Mizuno, H. Iwata, H. Takagi, S. Yoshikawa, Y. Umeda, Y. Matsuno, Y. Mori and H. Takemura, "Sonoporation with Doxorubicin Enhances Suppression of Intimal Hyperplasia in a Vein Graft Model," *The Journal of Surgical Research,* vol. 124, pp. 312-317, 2005.

[130] Y. Sakakima, S. Hayashi, Y. Yagi, A. Hayakawa, K. Tachibana and A. Nakao, "Gene Therapy for Haptocellular Carcinoma using Sonoporation Enhanced by Contrast Agents," *Cancer Gene Therapy,* vol. 12, p. 884, 2005.

[131] M. Nakashima, K. Tachibana, K. Iohara, M. Ito, M. Ishikawa and A. Akamine, "Induction of Reparative Dentin Formation by Ultrasound-Mediated Gene Delivery of Growth/Differentiation Factor 11," *Human Gene Therapy,* vol. 14, pp. 591-597, 2003.

[132] Y. Yamashita, M. Shimada, K. Tachibana, N. Harimoto, E. Tsujita, K. Shirabe, J. Miyazaki and K. Sugmachi, "In Vivo Gene Transfer into Muscle via Electro-Sonoporation," *Human Gene Therapy,* vol. 13, pp. 2079-2084, 2002.

[133] JoVE Science Education Database, *Basic Methods in Cellular and Molecular Biology,* Cambridge, MA: JoVE, 2017.

[134] Human Fertilisation & Embryology Authority, "Intracytoplasmic Sperm Injection," [Online]. Available: https://www.hfea.gov.uk/treatments/explore-all-treatments/intracytoplasmic-sperm-injection-icsi/. [Accessed July 2017].

[135] T. Huang, Interviewee, *Interview with Dr.Thomas Huang of the Pacific In Vitro Fertilization Institute.* [Interview]. 16 July 2017.

[136] K. M. Matthews, M. A. Rahman, M. Garcia and A. Ohta, "Rapid Measurement of Impedance Changes Associated with Developmental Phases in *Artemia* Cysts," in *Nano/Micro Engineered and Molecular Systems*, Los Angeles, 2017.

[137] K. Cheung, S. Gawad and P. Renaud, "Impedance Spectroscopy Flow Cytometry: On-Chip Label-Free Cell Differentiation," *Cytometry Part A,* vol. 65A, no. 2, pp. 124-132, 2005.

[138] P. Simon, M. Frankowski, N. Bock and J. Neukammer, "Label-Free Whole Blood Cell Differentiation Based on Multiple Frequency AC Impedance and Light Scattering Analysis in a Micro Flow Cytometer," *Lab on a Chip,* vol. 16, no. 12, pp. 2326-2338, 2016.

[139] H. Song, J. Rosano, Y. Wang, C. Garson, B. Prabhakarpandian, K. Pant, G. Klarmann, A. Perantoni, L. Alvarezbc and E. Laide, "Identification of Mesenchymal Stem Cell Differentiation State Using

Dual-Micropore Microfluidic Impedance Flow Cytometry," *Analytical Methods,* vol. 8, no. 41, pp. 7437-7444, 2016.

[140] J. Chen, X. Chengcheng, Y. Zhao, D. Chen, M.-H. Wu and J. Wang, "Microfluidic Impedance Flow Cytometry Enabling High-Throughput Single-Cell electrical Property Characterization," *International Journal of Molecular Sciences,* vol. 16, no. 5, pp. 9804-9830, 2015.

[141] P. Lavens and P. Sorgeloos, "The Cryptobiotic State of Artemia Cysts, its Diapause Deactivation and Hatching: A Review," in *Artemia Research and its Applications*, 1987.

[142] S. Gawad, L. Schild and P. Renaud, "Micromachined Impedance Spectroscopy Flow Cytometer for Cell Analysis and Particle Sizing," *Lab on a Chip,* vol. 1, pp. 76-82, 2001.

[143] T. B. Jones, Electromechanics of Particles, Cambridge: Cambridge University Press, 1995.

[144] K. Haubert, T. Drier and D. Beebe, "PDMS Bonding by Means of a Portable, Low-Cost Corona System," *Lab on a Chip,* vol. 6, no. 12, pp. 1548-1549, 2006.

[145] J. S. Clegg, "Protein Stability in Artemia Embryos During Prolonged Anoxia," *The Biological Bulletin,* vol. 212, no. 1, pp. 74-81, 2007.

[146] T. H. MacRae, "Stress Tolerance During Diapause and Quiescence of the Brine Shrimp, Artemia," *Cell Stress Chaperones,* vol. 21, no. 9, pp. 9-18, 2016.

[147] J. Podrabsky and S. Hand, "Physiological Strategies During Animal Diapause: Lessons from Brine Shrimp and Annual Killifish," *Journal of Experimental Biology,* vol. 218, no. 12, pp. 1897-1906, 2015.

[148] N. Gostling, X. Dong and P. Donoghue, "Ontogeny and Taphonomy: An Experimental Taphonomy Study of the Development of the Brine Shrimp Artemia Salina," *Palaeontology,* vol. 52, no. 1, pp. 169-186, 2009.

[149] M. Dumitrascu, "Artemia Salina," *Balneo-Research Journal,* vol. 2, no. 4, pp. 119-122, 2011.

[150] P. Lavens and P. Sorgeloos, Manual on the Production and Use of Live Food for Aquaculture, Rome: Food and Agriculture Organization of the United Nations, 1996.

[151] F. Bruni, G. Careri and J. Clegg, "Dielectric Properties of Artemia Cysts at Low Water Contents. Evidence for a Percolative Transistion," *Biophysical Journal,* vol. 55, no. 2, pp. 331-338, 1989.

[152] K. H. Schoenbach, F. E. Peterkin, S. Beebe, D. Byars, R. Alden, P. Adolphson and T. Turner, "Effect of Submicrosecond Electric Fields on Microorganisms: Experiments and Applications," in *Proceedings of SPIE, Novel Applications of Lasers and Pulsed Power*, San Jose, 1995.

[153] S. Kotopoulis, G. Dimcevski, O. Gilja, D. Hoem and M. Postema, "Treatment of Human Pancreatic Cancer Using Combined Ultrasound, Microbubbles, and Gemcitabine: A Clinical Use Study," *Medical Physics,* p. 072902, 2013.

[154] T. Linbo, *Zebrafish (Danio rerio) Husbandry and Colony Maintenance at the Northwest Fisheries Science Center,* US Department of Commerce, NOAA Technical Memorandum, NMFS-NWFSC-100, 62 p, 2009.